The Coupled Electron-Ion Monte Carlo Method

C. Pierleoni[1] and D.M. Ceperley[2]

[1] Department of Physics, University of L'Aquila, Polo di Coppito, Via Vetoio, L'Aquila, 67010 Italy
carlo.pierleoni@aquila.infn.it
[2] Department of Physics and NCSA, University of Illinois at Urbana-Champaign, Urbana, IL 61801, U.S.A.
david.ceperley@uiuc.edu

Carlo Pierleoni

C. Pierleoni and D.M. Ceperley: *The Coupled Electron-Ion Monte Carlo Method*, Lect. Notes Phys. **703**, 641–683 (2006)
DOI 10.1007/3-540-35273-2_18

1 Introduction 643

2 The Electronic Ground State Problem 644

2.1 Variational QMC 645
2.2 Reptation Quantum Monte Carlo 647
2.3 Fermions 652
2.4 Trial Wave Functions for Hydrogen 656
2.5 Twist Average Boundary Conditions 662
2.6 Sampling Electronic States: The "Bounce" Algorithm 663

3 Sampling Ionic States: The Penalty Method 666

3.1 Efficient Strategies for Electronic Energy Differences 668
3.2 Pre-Rejection 669

4 Quantum Protons 670

5 Summary of Results on High Pressure Hydrogen 673

6 Conclusions and Future Developments 679

References 680

1 Introduction

Twenty years ago Car and Parrinello introduced an efficient method to perform Molecular Dynamics simulation for classical nuclei with forces computed on the "fly" by a Density Functional Theory (DFT) based electronic calculation [1]. Because the method allowed study of the statistical mechanics of classical nuclei with many-body electronic interactions, it opened the way for the use of simulation methods for realistic systems with an accuracy well beyond the limits of available effective force fields. In the last twenty years, the number of applications of the Car-Parrinello ab-initio molecular dynamics has ranged from simple covalent bonded solids, to high pressure physics, material science and biological systems. There have also been extensions of the original algorithm to simulate systems at constant temperature and constant pressure [2], finite temperature effects for the electrons [3], and quantum nuclei [4].

DFT is, in principle, an exact theory but the energy functional are treated approximately at the level of a self consistent mean field theory for practical purposes. Despite recent progress, DFT suffers from well-known limitations, for example, excited state properties such as optical gaps and spectra are generally unreliable. DFT shows serious deficiencies in describing van der Waals interactions, non-equilibrium geometries such as reaction barriers, systems with transition metals and/or cluster isomers with competing bonding patterns [5, 6]. As a consequence, current ab-initio predictions of metallization transitions at high pressures, or even the prediction of phase transitions are often only qualitative. Hydrogen is an extreme case [7–9] but even in silicon the diamond/β-tin transition pressure and the melting temperature are seriously underestimated [10].

An alternative route to the ground state properties of a system of many electrons in presence of nuclei is the Quantum Monte Carlo method (QMC) [6, 11]. QMC methods for bosons are "exact" meaning that all systematic errors are under control and can be reduced as much as desired with a computational cost growing as a power of the number of particles. However for fermions the "sign problem" makes a direct extension of QMC unstable and one has to resort to the "fixed node approximation" for practical calculations [6, 11]. Over the years, the level of accuracy of the fixed node approximation for simple homogeneous systems, such as ^{3}He and the electron gas, has been systematically improved [12–14]. In more complex, inhomogeneous situations such as atoms, molecules and extended systems of electrons and nuclei, progress have been somewhat slower. Nonetheless, in most cases, fixed-node QMC methods have proved to be more accurate than mean field methods (HF and DFT) [6]. Computing ionic forces with QMC to replace the DFT forces in the ab-initio MD, is more difficult and a general and efficient algorithm is still missing. Moreover, the computer time required for a QMC estimate of the electronic energy is, in general, more than for a corresponding DFT-LDA calculation. These problems have seriously limited the development of

an ab-initio simulation method based on the QMC solution of the electronic problem "on the fly".

In recent years, we have developed a different strategy based entirely on the Monte Carlo method, both for solving the electronic problem, and for sampling the ionic configuration space [15, 16]. The new method, called the Coupled Electron-Ion Monte Carlo method (CEIMC) relies on the Born-Oppenheimer approximation for treating finite temperature ions coupled with ground state electrons. A Metropolis Monte Carlo simulation of the ionic degrees of freedom (represented either by classical point particles or by path integrals) at fixed temperature is performed based on the electronic energies computed during independent ground state Quantum Monte Carlo calculations. CEIMC has been applied, so far, to high pressure metallic hydrogen where it has found quite different effects of temperature than CPMD with Local Density Approximation (LDA) forces [17]. In this chapter, we present the theoretical basis of CEIMC. We start by describing, in some detail, the ground state QMC methods implemented in CEIMC, namely the Variational Monte Carlo and the Reptation Quantum Monte Carlo methods. We then describe the fixed node or restricted paths approximation necessary to treat fermions and the fixed phase method used to perform the average over boundary conditions needed for metallic system. In the subsequent section we describe how to implement the Metropolis algorithm when the energy difference has a statistical noise and discuss efficient strategies for energy differences within the CEIMC. The next section is devoted to describe the method to treat quantum mechanical protons and to integrate efficiently this new difficulty within CEIMC. Finally, we briefly review some CEIMC results for high pressure hydrogen and compare with existing CPMD results. Conclusions and perspectives for future developments are collected in the last section.

2 The Electronic Ground State Problem

Let us consider a system of N_p nuclei and N_e electrons in a volume V described by the non relativistic Hamiltonian

$$\hat{H} = -\sum_{i=1}^{N} \lambda_i \nabla_i^2 + \frac{e^2}{2} \sum_{i \neq j}^{N} \frac{z_i z_j}{|\hat{\boldsymbol{r}}_i - \hat{\boldsymbol{r}}_j|} \tag{1}$$

where $N = N_e + N_p$, and z_i, m_i, $\hat{\boldsymbol{r}}_i$ represent the charge, mass and position operator of particle i respectively and $\lambda_i = \hbar^2/2m_i$. Let us denote with $R = (\boldsymbol{r}_1, \ldots, \boldsymbol{r}_{N_e})$ and $S = (\boldsymbol{r}_{N_e+1}, \ldots, \boldsymbol{r}_N)$ the set of coordinates of all electrons and nuclei respectively. We restrict the discussion to unpolarized systems, i.e. systems with a vanishing projection of the total spin along a given direction, say $S_z = 0$. Since the Hamiltonian does not flip spins, we can label electrons from 1 to $N_e/2$ as up spin ($\uparrow$) and electrons from $N_e/2 + 1$ to N_e as down spin ($\downarrow$).

Within the Born-Oppenheimer approximation, the energy of the system for a given nuclear state S is the expectation value of the Hamiltonian $\hat{H}$ over the corresponding exact ground state $|\Phi_0(S)\rangle$

$$E_{BO}(S) = \langle \Phi_0(S)|\hat{H}|\Phi_0(S)\rangle \tag{2}$$

which is a $3N_e$ dimensional integral over the electronic coordinates in configurational space

$$E_{BO}(S) = \int dR\, \Phi_0^*(R|S)\hat{H}(R,S)\Phi_0(R|S) = \int dR\, |\Phi_0(R|S)|^2\, E_L(R|S) \tag{3}$$

with the *local energy* defined as

$$E_L(R|S) = \frac{\hat{H}(R,S)\Phi_0(R|S)}{\Phi_0(R|S)} \tag{4}$$

Since $\Phi_0(R|S)$ is normalized and $|\Phi_0(R|S)|^2 \geq 0$ everywhere, the $3N_e$ dimensional integral in (3) can be performed by standard Metropolis Monte Carlo by generating a Markov process which sample asymptotically $|\Phi_0(R|S)|^2$. Expectation values of any observable can be computed along the same Markov chain. In this respect, computing the properties of a many-body quantum system is similar to performing a MC calculation for a classical system. The square modulus of the ground state wave function plays the role of the classical Boltzmann distribution. An important quantity in what follows is the measure of the energy fluctuations for a given wave function. This can be defined by the variance of the local energy

$$\begin{aligned}\sigma^2(S) &= \int dR\, |\Phi_0(R|S)|^2 \left(\frac{\hat{H}(R,S)\Phi_0(R|S)}{\Phi_0(R|S)} - E_{BO}(S) \right)^2 \\ &= \int dR \left(\hat{H}\Phi_0(R|S) \right)^2 - E_{BO}^2(S)\end{aligned} \tag{5}$$

Note that for any exact eigenfunction of the hamiltonian, the local energy $E_L(R|S)$ does not depend on the electronic configuration R and is equal to the corresponding eigenvalue. This implies that the variance vanishes. This is known as the zero variance principle in Quantum Monte Carlo.

2.1 Variational QMC

The problem is to get a computable expression for the ground state wave function without solving the Schrödinger equation for the many body hamiltonian of (1), obviously an impossible task for any non trivial system. As usual in many body problems, we can resort to the variational principle which states that the energy of any proper trial state $|\Psi_T(S)\rangle$ will be greater or equal to the ground state energy

$$E_{BO}(S) \leq E_V(S) = \frac{\int dR\ \Psi_T^*(R|S)\hat{H}(R,S)\Psi_T(R|S)}{\int dR\ \Psi_T^*(R|S)\Psi_T(R|S)} \tag{6}$$

A proper trial wave function must satisfy the following requirements

- it has to have the right symmetry under particle permutation: $\Psi_T(\hat{P}R|S) = (-1)^P\Psi_T(R|S)$, where $\hat{P}$ is the permutation operator for electrons of same spin.
- the quantity $\hat{H}\Psi_T$ needs to be well defined everywhere which implies that both Ψ_T and $\nabla\Psi_T$ must be continuous whenever the potential is finite, including at the periodic boundaries.
- the integrals $\int dR|\Psi_T|^2$ and $\int dR\Psi_T^*\hat{H}\Psi_T$ must exist. Furthermore for a Monte Carlo evaluation of the variance σ^2 the integral $\int dR(\hat{H}\Psi_T)^2$is also required to exist.

For a given trial function, it is essential to show analytically that these properties hold everywhere, in particular at the edge of the periodic box and when two particles approach each other (where generally the potential diverges). Otherwise, either the upper bound property is not guaranteed or the Monte Carlo error estimates are not valid.

The strategy in Variational Monte Carlo (VMC) is therefore to pick a proper form for a trial wave function based on physical insight for the particular system under study. In general, a number of parameters $(\alpha_1, \ldots, \alpha_k)$ will appear in the wave function to be treated as variational parameters. For any given set of $\{\alpha\}$ the Metropolis algorithm is used to sample the distribution

$$\Pi(R|S,\{\alpha\}) = \frac{\Psi_T(R|S,\{\alpha\})}{\int dR\Psi_T(R|S,\{\alpha\})} \tag{7}$$

and the electronic properties are then computed as averages over the generated Markov chain

$$E_V^T(S,\{\alpha\}) = \langle\ E_L(R|S,\{\alpha\})\ \rangle \tag{8}$$

where the superscript T as been explicitly written to remember that the variational energy depends in general on the chosen analytical form and, for any given form, on the numerical values of the variational parameters $\{\alpha\}$.

Because of the zero variance principle stated above, the fluctuations in the local energy are entirely due to inaccuracies of the trial function for the particular configurations generated during the MC run. As the trial wave function approaches the exact eigenfunction (everywhere in configuration space!) the fluctuations decrease and the variational estimate of the energy converges more rapidly with the number of MC steps. At the same time, the estimate converges to the exact energy. This is at variance with classical Monte Carlo where fluctuations are induced by temperature.

The variational method is very powerful, and intuitively pleasing. One posits a form of the trial function and then obtains an upper bound for the energy. In contrast to other theoretical methods, no further approximations

are made. The only restriction on the trial function is to be computable in a reasonable amount of time.

One of the problems with VMC is that it favors simple states over more complicated states. As an example, consider the liquid-solid transition in helium at zero temperature. The solid wave function is simpler than the liquid wave function because in the solid the particles are localized so that the phase space that the atoms explore is much reduced. This biases the difference between the liquid and solid variational energies for the same type of trial function, (e.g. a pair product form, see below) since the solid energy will be closer to the exact result than the liquid. Hence, the transition density will be systematically lower than the experimental value. Another illustration is the calculation of the polarization energy of liquid ^{3}He. The wave function for fully polarized helium is simpler than for unpolarized helium because antisymmetry requirements are higher in the polarized phase so that the spin susceptibility computed at the pair product level has the wrong sign!

The optimization of trial functions for many-body systems is time consuming, particularly for complex trial functions. The dimension of the parameter space increases rapidly with the complexity of the system and the optimization can become very cumbersome since it is, in general, a nonlinear optimization problem. Here we are not speaking of the computer time, but of the human time to decide which terms to add, to program them and their derivatives in the VMC code. This allows an element of human bias into VMC; the VMC optimization is more likely to be stopped when the expected result is obtained. The basis set problem is still plaguing quantum chemistry even at the SCF level where one only has 1-body orbitals. VMC shares this difficulty with basis sets as the problems get more complex.

Finally, the variational energy is insensitive to long range order. The energy is dominated by the local order (nearest neighbor correlation functions). If one is trying to compare the variational energy of a trial function with and without long range order, it is extremely important that both functions have the same short-range flexibility and both trial functions are equally optimized locally. Only if this is done, can one have any hope of saying anything about the long range order. The error in the variational energy is second order in the trial function, while any other property will be first order. Thus variational energies can be quite accurate while correlation functions are not very accurate.

As a consequence, the results typically reflect what was put into the trial function. Consider calculating the momentum distribution. Suppose the trial function has a Fermi surface. Then the momentum distribution will exhibits a discontinuity at k_f signaling the presence of a Fermi surface. This does not imply that the true wave function has a sharp Fermi surface.

2.2 Reptation Quantum Monte Carlo

It is possible to go beyond VMC by a number of related methods known as Projection Monte Carlo Methods. The general idea is to chose a trial function

which has a non negligible overlap with the ground state wave function (in general, it is enough to require the right symmetry) and to apply a suitable projection operator which zeros out all the components of the trial wave function from the excited states in the Hilbert space of the system. We will limit the description to the method implemented in CEIMC, namely the Reptation Quantum Monte Carlo [18] or Variational Path Integral [19, 20]. For the discussion of other projection QMC methods such as Diffusion Monte Carlo (DMC) and Green Function Monte Carlo (GFMC), we refer to the specialized literature [6, 11].

Let us define $\{\Phi_i, E_i\}$ as the complete set of eigenfunctions and eigenvalues of the hamiltonian $\hat{H}$ in (1). Any trial state can be decomposed in the eigenstate basis:

$$|\Psi_T\rangle = \sum_i c_i |\Phi_i\rangle \tag{9}$$

where c_i is the overlap of the trial state with the i^{th} eigenstate. Let us consider the application of the operator $e^{-t\hat{H}}$ onto this state

$$|\Psi(t)\rangle = e^{-t\hat{H}}|\Psi(0)\rangle = \sum_i c_i e^{-tE_i}|\Phi_i\rangle \tag{10}$$

with the initial state $|\Psi(0)\rangle = |\Psi_T\rangle$. Here t is a control parameter with dimension of inverse energy and we will call it "time" since it plays the role of imaginary time in the Bloch equation (see below). All excited states will be zeroed exponentially fast with increasing t, the rate of the convergence to the ground state depending on the energy gap between the ground state and the first excited state non-orthogonal to the trial function. The total energy as function of time is defined as

$$E(t) = \frac{\langle \Psi(t/2)|\hat{H}|\Psi(t/2)\rangle}{\langle \Psi(t/2)|\Psi(t/2)\rangle} = \frac{\langle \Psi_T|e^{-\frac{t}{2}\hat{H}}\hat{H}e^{-\frac{t}{2}\hat{H}}|\Psi_T\rangle}{\langle \Psi_T|e^{-t\hat{H}}|\Psi_T\rangle} \tag{11}$$

Similar to a thermal partition function, let us define the generating function of the moments of $\hat{H}$ as

$$Z(t) = \langle \Psi_T|e^{-t\hat{H}}|\Psi_T\rangle \ . \tag{12}$$

The total energy at time t is simply the derivative of the logarithm of $Z(t)$

$$E(t) = -\frac{\partial}{\partial t} ln Z(t) \tag{13}$$

and the variance of the energy is the second derivative

$$\sigma_E^2(t) = \langle (\hat{H} - E(t))^2 \rangle = -\frac{\partial}{\partial t} E(t) \geq 0 \tag{14}$$

which is non-negative by definition. This implies that the energy decreases monotonically with time. The ground state is reached at large time (much larger than the inverse gap) and

$$\lim_{t\to\infty} E(t) = E_0 \tag{15}$$

$$\lim_{t\to\infty} \sigma^2(t) = 0 \tag{16}$$

The last relation is the generalization of the zero variance principle in Projection Monte Carlo.

For observables $\hat{A}$ which do not commute with $\hat{H}$, for instance correlation functions, the average at "time" t, defined as in (11), takes the following form in configurational space[3]

$$A(t) = \langle\, \hat{A} \,\rangle_t = \frac{1}{Z(t)} \int dR_1 dR_2 dR_3 dR_4 \,\langle\, \Psi_T | R_1 \,\rangle\, \rho\left(R_1, R_2 | \frac{t}{2}\right) \langle\, R_2 | \hat{A} | R_3 \,\rangle\, \rho(R_3, R_4 | \frac{t}{2}) \,\langle\, R_4 | \Psi_T \,\rangle \tag{17}$$

where R_i represent the set of all electronic coordinates and $\rho(R, R', t)$ is the thermal density matrix of the system at inverse temperature t

$$\rho(R, R', t) = \langle\, R | e^{-t\hat{H}} | R' \,\rangle \tag{18}$$

Similarly, the expression of $Z(t)$ in configurational space is

$$Z(t) = \int dR_1 dR_2 \,\langle\, \Psi_T | R_1 \,\rangle\, \rho(R_1, R_2, t) \,\langle\, R_2 | \Psi_T \,\rangle \tag{19}$$

Thus, in order to compute any average over the ground state we need to know the thermal density matrix at large enough "time". Obviously, its analytic form for any non-trivial many-body system is unknown. However, at short time (or high temperature) the system approaches its classical limit and we can obtain approximations. Let us first decompose the time interval t in M smaller time intervals, $\tau = t/M$

$$\rho(R, R', t) = \langle\, R | e^{-(\tau\hat{H})^M} | R' \,\rangle = \int dR_1 \cdots dR_{M-1} \prod_{k=1}^{M-1} \langle\, R_{k-1} | e^{-\tau\hat{H}} | R_k \,\rangle \tag{20}$$

with the boundary conditions: $R_0 = R$ and $R_M = R'$ on the paths. For M large enough, we can apply the Trotter factorization to get an explicit form for the short time propagator. The simplest factorization, known as the "primitive" approximation, consists of ignoring the commutator of the kinetic and potential operators

$$\rho(R_{k-1}, R_k, \tau) = \langle\, R_{k-1} | e^{-\tau\hat{H}} | R_k \,\rangle \simeq \langle\, R_{k-1} | e^{-\tau\hat{K}} | R_k \,\rangle\, e^{-\frac{\tau}{2}[V(R_k)+V(R_{k-1})]} \tag{21}$$

[3] The expression gets slightly easier for observables diagonal in configurational space: $\langle\, R | A | R' \,\rangle = A(R)\delta(R - R')$.

A more accurate, but also more complex form, will be discussed later in the section on Path Integral Monte Carlo. Note that we have symmetrized the primitive form in order to reduce the systematic error of the factorization [19]. The explicit form of the kinetic propagator is the Green's function of the Bloch equation of a system of free particles [19, 21], i.e. a diffusion equation in configurational space

$$\langle\, R_{k-1}|e^{-\tau\hat{K}}|R_k\,\rangle = \left(\frac{1}{4\pi\lambda\tau}\right)^{\frac{3N}{2}} e^{-\frac{|R_k-R_{k-1}|^2}{4\lambda\tau}} \tag{22}$$

and therefore we get

$$\rho(R,R',t) = \int \prod_{k=1}^{M-1} dR_k \left[\prod_{k=1}^{M} \frac{e^{-\frac{|R_k-R_{k-1}|^2}{4\lambda\tau}}}{(4\pi\lambda\tau)^{3N/2}}\right] e^{-\tau\left[\frac{V(R_0)}{2}+\sum_{k=1}^{M-1}V(R_k)+\frac{V(R_M)}{2}\right]} \tag{23}$$

In the continuous limit ($M \to \infty$, $\tau \to 0$, $t = M\tau = \text{const.}$) it becomes the Feynman-Kac formula [19]

$$\rho(R,R',t) = \left\langle \exp\left(-\int_0^t d\tau V(R(\tau))\right)\right\rangle_{RW} \tag{24}$$

where $\langle \cdots \rangle_{RW}$ indicate a path average over gaussian random walks $R(\tau)$ starting at $R(0) = R$ and ending at $R(t) = R'$ in a time t.

We have, in principle, developed a scheme for Monte Carlo calculations of ground state averages of a general quantum system. However, this scheme has a serious problem of efficiency which prevents its use for any non-trivial system. At the origin of the problem are the wild variations of the potential $V(R)$ in configuration space. There are cases like electron-proton systems where the potential is not bounded and therefore the primitive approximation of the propagator is not stable for any finite time step τ. However, even with well behaved effective potentials (like in Helium for instance) the large fluctuations of the potential energy would require a very small time step in order to observe convergence of the averages to their exact value. Moreover, the efficiency will degrade rapidly with more particles. The problem was recognized in the early days of QMC and the remedy introduced by Kalos in 1974. In the community of Ground State QMC it goes under the name of "importance sampling" (IS). A different strategy is applied in the PIMC community. We now describe importance sampling, not in the original form as introduced by Kalos in Green's Function Monte Carlo, but following a recent development by Baroni and Moroni in the framework of the Reptation QMC [18].

In VMC, a good trial function should have a local energy almost constant in configuration space. Let us assume to know such function Ψ_T. Let us then rewrite the hamiltonian $\hat{H}$ in terms of a new fictitious hamiltonian $\hat{\mathcal{H}}$

$$\hat{H} = \hat{\mathcal{H}} + E_L(R) \tag{25}$$

where

$$\hat{\mathcal{H}} = \lambda \left[-\nabla^2 + \frac{\nabla^2 \Psi_T}{\Psi_T} \right] \tag{26}$$

$$E_L(R) = V(R) - \lambda \frac{\nabla^2 \Psi_T}{\Psi_T} \tag{27}$$

We can now factorize the short time propagator in a different way (confr. (21))

$$\rho(R_{k-1}, R_k, \tau) \simeq \langle\, R_{k-1} | e^{-\tau \hat{\mathcal{H}}} | R_k \,\rangle\; e^{-\frac{\tau}{2}[E_L(R_k) + E_L(R_{k-1})]} \tag{28}$$

In this new form, the widely oscillating potential energy is replaced by the local energy which is much smoother for an accurate Ψ_T. We need to find the short time propagator of the importance sampling hamiltonian $\hat{\mathcal{H}}$ which is nothing but the solution of the corresponding Bloch equation [19, 21]

$$-\partial_t \rho_{IS}(R, R', t) = \hat{\mathcal{H}} \rho_{IS}(R, R', t) \tag{29}$$

$$\rho_{IS}(R, R', 0) = \delta(R - R') \tag{30}$$

It is not difficult to show by direct substitution, that the short time solution of this equation is

$$\rho_{IS}(R_{k-1}, R_k, \tau) = \frac{\Psi_T(R_{k-1})}{\Psi_T(R_k)} \left(\frac{1}{4\pi\lambda\tau} \right)^{\frac{3N}{2}} \exp\left\{ -\frac{(R_k - R_{k-1} - 2\lambda\tau F_{k-1})^2}{4\lambda\tau} \right\} \tag{31}$$

if we make the short time approximation $\left[1 + \tau \left(\nabla F + \frac{1}{F}\nabla^2 F\right) \simeq 1\right]$. In these expressions, the drift force is defined as $F_k = F(R_k) = 2\nabla_{R_k} \ln \Psi_T(R_k)$.

This form of the short time propagator does not satisfy an important property of density matrices, namely the symmetry under exchange of the two legs, R and R'. We can remedy by taking the symmetrized density matrix as short time propagator

$$\rho^s_{IS}(R_{k-1}, R_k, \tau) = [\rho_{IS}(R_{k-1}, R_k, \tau)\rho_{IS}(R_k, R_{k-1}, \tau)]^{\frac{1}{2}} = \frac{e^{-L_s(R_{k-1}, R_k, \tau)}}{(4\pi\lambda\tau)^{\frac{3N}{2}}} \tag{32}$$

where the expression for the symmetrized link action is

$$L_s(R_{k-1}, R_k, \tau) = \frac{(R_k - R_{k-1})^2}{4\lambda\tau} + \frac{\lambda\tau}{2}(F_k^2 + F_{k-1}^2) + \frac{(R_k - R_{k-1}) \cdot (F_k - F_{k-1})}{2} \tag{33}$$

Using (32), (33) we obtain the propagator at any time t as

$$\rho(R, R', t) = \int \prod_{k=1}^{M-1} dR_k \left[\prod_{k=1}^{M} \frac{e^{-L_s(R_{k-1}, R_k, \tau)}}{(4\pi\lambda\tau)^{3N/2}} \right] e^{-\tau\left[\frac{E_L(R_0)}{2} + \sum_{k=1}^{M-1} E_L(R_k) + \frac{E_L(R_M)}{2}\right]} \tag{34}$$

In the continuum limit it is the generalized Feynman-Kac formula

$$\rho(R,R',t) = \left\langle \exp\left(-\int_0^t d\tau E_L(R(\tau))\right)\right\rangle_{DRW} \tag{35}$$

where $\langle \cdots \rangle_{DRW}$ indicate a path average over drifted random walks starting at $R(0) = R$ and ending at $R(t) = R'$ in a time t. With this form of the density matrix the generating function takes the form

$$Z(t) = \int dRdR' \Psi_T(R) \left\langle e^{-\int_0^t d\tau E_L(R(\tau))}\right\rangle_{DRW} \Psi_T(R') \tag{36}$$

and the average of a generic observable $\hat{A}$ becomes

$$A(t) = \frac{1}{Z(t)} \int \prod_{k=1}^{4} dR_k \Psi_T(R_1) \left\langle e^{-\int_0^{\frac{t}{2}} d\tau E_L(R(\tau))}\right\rangle_{DRW} A(R_2,R_3) \left\langle e^{-\int_0^{\frac{t}{2}} d\tau E_L(R(\tau))}\right\rangle_{DRW} \Psi_T(R_4) \tag{37}$$

with obvious boundary conditions on the path averages.

A special word on the calculation of the energy is in order. In the last equality in (11) the hamiltonian operator in the numerator can be pushed either to the left or to the right in such a way to operate directly on the trial state. Remembering the definition of the local energy, (4), we can write

$$\begin{aligned} E(t) &= \frac{1}{Z(t)} \int dRdR' E_L(R) \Psi_T(R) \rho(R,R',t) \Psi(R') \\ &= \frac{1}{Z(t)} \int dRdR' \Psi_T(R) \rho(R,R',t) \Psi(R') E_L(R') \\ &= \frac{1}{2} \left\langle E_L(R) + E_L(R') \right\rangle \end{aligned} \tag{38}$$

We use the last equality in order to improve the efficiency of the estimator. When computing the variance we push one $\hat{H}$ operator to the left and the other to the right to obtain

$$\sigma^2(t) = \int dRdR' E_L(R) \Psi_T(R) \rho(R,R',t) \Psi(R') E_L(R') - E^2(t) \tag{39}$$

Then reaching the ground state with vanishing variance means taking paths long enough (t large enough) for the correlation between the two ends to vanish. On the other hand the VMC method is obtained for $t = 0$ as $\rho(R,R',0) = \delta(R-R')$.

2.3 Fermions

Up to now we have tacitly ignored the particle statistics and derived the formalism as if the particles were distinguishable. As far as the Hamiltonian

does not depend explicitly on spin, the formalism remains valid for fermions if we consider states completely antisymmetric under particle permutation $|\hat{P}R_i\rangle = (-)^P|R_i\rangle$. The importance sampling hamiltonian $\hat{\mathcal{H}}$, defined in the same way, is symmetric under particle exchange even for antisymmetric trial states. The only place where we need care is in the initial condition of the Bloch equation, (30), which must be replaced by a completely antisymmetric delta function

$$\rho_{IS}(R, R', 0) = \mathcal{A}\delta(R - R') = \frac{1}{N!}\sum_P (-1)^P \delta(R - \hat{P}R') \tag{40}$$

Since $[\hat{H}, \hat{P}] = 0$, the imaginary time evolution preserves the symmetry and the fermion thermal density matrix takes the form

$$\rho_F(R, R', t) = \frac{1}{N!}\sum_P (-1)^P \rho_D(R, \hat{P}R', t) \tag{41}$$

where ρ_D is the density matrix of a system of distinguishable particles derived above (see (35)). The fermion density matrix between configurations R and R' at "time" t is the sum over permutations of the density matrix of distinguishable particles between the initial configurations R and the permutation of the final configuration $\hat{P}R'$, multiplied by the sign of the permutation. Each of those density matrices arises from the sum over all paths with given boundary conditions in time as expressed by the generalized Feynman-Kac formula. We can therefore think of a path in the configurational space of distinguishable particles as an object carrying not only a weight (given by the exponential of minus the integral of the local energy along the path) but also a sign fixed by its boundary conditions in time. The fermion density matrix is the algebraic sum over all those paths. While $\rho_D(R, R', t) \geq 0$ for any R' and t at given R, this property obviously does not apply to $\rho_F(R, R', t)$. This is at the origin of the "fermion sign problem" [26]. Briefly, the sign problem arises from the fact that the optimal probability to sample the electronic paths is the absolute value of the fermion density matrix which, however, is a bosonic density matrix (symmetric under particle permutation). With this sampling, the sign of the sampled paths will be left in the estimator for the averages. The normalization of any average will be given by the number of sampled positive paths minus the number of sampled negative paths. Since the sampling is bosonic, i.e. symmetric, these two numbers will eventually be equal and the noise on any average will blow up for a long enough sampling. The fundamental reason behind this pathology is that the Hilbert space of any time independent Hamiltonian (with local interactions) can be divided in the set of symmetric states, antisymmetric states and states of mixed symmetry. These sets are disjoint, e.g. any symmetric state is orthogonal to any antisymmetric one; in principle we cannot extract information for a fermionic state from a bosonic sampling [22].

A general solution of the fermion sign problem is still unavailable, although interesting algorithms have been proposed [11]. A class of methods try to

build the antisymmetry constraint into the propagator, while other methods try to reformulate the problem of sampling in the space of antisymmetric wavefunctions (determinants) [23–25]. All these "fermions" methods are still at an early stage and their application has been limited so far to quite small numbers of fermions. The more robust and widely used, although approximate, method is the so-called restricted path or fixed node method [6, 26].

Within the fixed-node method, we need to consider the nodal surfaces of the fermion density matrix. For any given configuration R, these are defined by the implicit equation $\rho_{_F}(R, R', t) = 0$, as the locations R' at which the density matrix at time t vanishes. The nodal surfaces of the initial configuration R divide the configurational space of R' in regions of positive $\rho_{_F}$ and regions of negative $\rho_{_F}$. In terms of individual paths, the nodal locations are hypersurfaces in configurational space on which the sum of contributions of the positive and negative paths to the density matrix vanishes. Since the fermion density matrix satisfies the usual convolution relation [21]

$$\rho_{_F}(R, R', t) = \int dR'' \rho_{_F}(R, R'', \tau)\rho_{_F}(R'', R', t - \tau) \qquad \forall \tau \in [0, t] \tag{42}$$

the configurations R'' belonging to the nodal surface of the initial point R at the arbitrary time τ will not contribute to the integral and therefore to the density matrix at any future time t. Therefore in constructing the fermion density matrix from R to R' at time t as sum over signed paths, we can safely disregard all those paths which have reached the nodal surface at any previous time $\tau \leq t$. If we define the reach of R at time t, $\Upsilon(R, t)$, as the set of points that can be reached from R in a time t without having crossed the nodal surfaces at previous times, the argument above can be formalized in the restricted paths identity[4]

$$\rho_{_F}(R, R', t) = \frac{1}{N!} \sum_P (-)^P \left(\int_{Y(0)=R, Y(t)=PR'} \mathcal{D}Y \; e^{-S[Y]} \right)_{\Upsilon(R,t)} \tag{43}$$

where $S[Y]$ represent the action of the generic path Y (see (34) for its discretized form). Let us now consider the generating function $Z(t)$ of (19). Using the restricted paths identity we obtain

$$\begin{aligned} Z(t) &= \int dR dR' \Psi_T(R) \frac{1}{N!} \sum_P (-)^P \left(\int_{Y(0)=R, Y(t)=PR'} \mathcal{D}Y \; e^{-S[Y]} \right)_{\Upsilon(R,t)} \Psi_T(R') \\ &= \int dR dR'' \Psi_T(R) \left(\int_{Y(0)=R, Y(t)=R''} \mathcal{D}Y \; e^{-S[Y]} \right)_{\Upsilon(R,t)} \frac{1}{N!} \sum_P (-)^P \Psi_T(P^{-1}R'') \\ &= \int dR dR'' \Psi_T(R) \left(\int_{Y(0)=R, Y(t)=R''} \mathcal{D}Y \; e^{-S[Y]} \right)_{\Upsilon(R,t)} \Psi_T(R'') \end{aligned} \tag{44}$$

[4] In [27] an alternative proof based on the Bloch equation is provided.

where in the last equality we have used the fact that the trial wave function is antisymmetric under particle permutations: $(-)^P \Psi_T(\hat{P}^{-1}R) = \Psi_T(R)$. In this last form the integrand is always positive since for each R, the functional integral is restricted to paths inside its reach so that $\Psi_T(R)\Psi_T(R') \geq 0$ (if the nodes of the trial function are correct). Therefore using the restricted path identity we have proven that the generating function is a positive function at any time t and can be computed considering only positive paths which do not cross the nodal surfaces.

The restricted paths identity is by no means the solution of the sign problem since in order to know the nodal surfaces we have to know the density matrix itself. However rephrasing the problem in terms of spacial boundary conditions can lead to interesting approximate schemes. The nodal surface of the fermion density matrix for a system of N interacting particles is a highly non-trivial function in 6N dimensions and not much is known about it [27,28]. The approximate method, known as fixed node in ground state QMC [6] and as restricted paths in PIMC [26], consists in replacing the nodal surfaces of the exact fermion density matrix with the nodal surfaces of some trial density matrix. In ground state QMC, it is customary to restrict the class of possible nodal surfaces to time independent nodes and, within this class, the most reasonable choice is to assume the nodes of the trial wave function Ψ_T. In practice, this step requires a very minor modification of the algorithm: it is enough to ensure that $\Psi_T(R_{k-1})\Psi_T(R_k) > 0$ for any time interval along the sampled paths. In the continuous limit this restriction will enforce the restricted path identity.

The nodal surfaces of the trial wave function divide the configurational space in disconnected regions. In order to perform the configurational integral over R and R' in (44) it could appear necessary to sample all nodal regions. However, it can be proved that the nodal regions of the ground state of any Hamiltonian with a reasonable local potential are all equivalent by symmetry (Tiling theorem) [27]. This "tiling" theorem ensures that computing in a single nodal region is equivalent to a global calculation.

A further important property of the Fixed node method is the existence of a variational theorem: the FN-RQMC energy is an upper bound of the true ground state energy $E_T(\infty) \geq E_0$, and the equality holds if the trial nodes coincide with the nodes of the exact ground state [6]. Therefore for fermions, even projection methods such as RQMC are variational with respect to the nodal positions; the nodes are not optimized by the projection mechanism. The "quality" of the nodal location is important to obtain accurate results.

In some cases it is necessary to consider complex trial functions, for instance in the presence of a magnetic field [29] or in the twist average method to be discussed later [30]. In these cases we have to deal with a trial function of the form

$$\Psi_T(R) = |\Psi_T(R)| e^{i\varphi_T(R)} \tag{45}$$

where $\varphi_{_T}(R)$, a real function, is the configuration dependent phase of the wave function. Obviously in VMC no differences arise in the use of complex trial functions other than in the estimators for the averages. For instance, the local energy is modified (confr. (27)) and contains an imaginary part

$$E_L(R) = V(R) - \lambda \frac{\nabla^2 |\Psi_T|}{|\Psi_T|} + \lambda \left(\nabla \varphi_{_T}\right)^2 - i\lambda \left(2\nabla \varphi_{_T} \frac{\nabla |\Psi_T|}{|\Psi_T|} + \nabla^2 \varphi_{_T} \right) \quad (46)$$

Here, we limit the discussion to systems with time-reversal symmetry, i.e. zero magnetic fields. As Ψ_T approaches the exact ground state, the local energy approaches a real constant equal to the ground state energy while the imaginary part of the local energy vanishes. It is therefore natural to take the real part of (46) as energy estimator and, in addition to the variance, to monitor the deviation of the imaginary part from zero as an indicator of the quality of the trial wave function.

How do we have to modify the RQMC to work with complex wave functions? For general complex functions Φ, we can split the time independent Schrödinger equation into two coupled equations, one for the modulus $|\Phi|$ and one for the phase φ of the wave function

$$\left\{ -\lambda \nabla^2 + \left[V(R) + \lambda (\nabla \varphi)^2 \right] \right\} |\Phi| = E |\Phi| \quad (47)$$

$$\nabla^2 \varphi + 2 \nabla \varphi \cdot \frac{\nabla |\Phi|}{|\Phi|} = 0 \quad (48)$$

In the "fixed phase" approximation [29, 31] one keeps the phase of the wave function $\varphi(R)$ fixed to some analytic form during the calculation, and solves the imaginary time dependent Schrödinger equation corresponding to the stationary problem of (47). Even for fermions this is a bosonic problem (since the modulus of the wave function must be symmetric under particle exchange) with a modified interaction $\left[V(R) + \lambda (\nabla \varphi)^2 \right]$. We can still perform the IS transformation and the formalism remains the same if the local energy is defined as the real part of (46). Note that the fixed node constraint for real trial functions can be recast into the fixed phase algorithm if we write $\varphi_{_T}(R) = \pi [1 - \theta(\frac{\Psi_T(R)}{|\Psi_T(R)|})]$ so that the phase of the trial function changes by π across the nodes at it should. Since the phase is a step function, its gradient is a δ function and provides an infinite contribution in the action of paths crossing the nodes, i.e. a vanishing probability to cross the nodes.

In this section we have not explicitly indicated the dependence on the ionic state S. In the BO approximation, ions play the role of external fields for the electronic system so that their coordinates appear explicitly in the Hamiltonian, in the trial state, in the local energy and in drift force for the IS procedure.

2.4 Trial Wave Functions for Hydrogen

In this subsection, we describe some general properties of the trial wave functions for electronic systems. We will restrict our discussion to the case of a

proton-electron system, i.e. hydrogen and refer to the literature for more complex systems (heavier elements) [6, 11]. In particular, we will not discuss the use of pseudopotentials in QMC and the related trial wave functions which, however, will be an important issue in future extensions of CEIMC.

The Pair Product Trial Function

The pair product trial wave function is the simplest extension of the Slater determinant of single particle orbitals used in mean field treatment of electronic systems (HF or DFT). This is also the ubiquitous form for trial functions in VMC

$$\Psi_{SJ}(R, \Sigma|S) = \exp\left(-\sum_{i<j} u_{ij}(r_{ij})\right) det[\theta_k(\boldsymbol{r}_i, \sigma_i|S)] \tag{49}$$

where $\Sigma = \{\sigma_1, \ldots, \sigma_{N_e}\}$ is the set of spin variables of the electrons, $\theta_k(\boldsymbol{r}, \sigma|S)$ is the k^{th} spin orbital for the given nuclear configuration and $\theta_k(\boldsymbol{r}_i, \sigma_i|S)$ is the Slater matrix. The additional term $u_{ij}(r_{ij})$ is the "pseudopotential" or pair correlation factor which introduces explicitly the two body correlations into the many body wave function. This term is of bosonic nature, i.e. is symmetric under particle exchange, while the antisymmetry is ensured by the determinant. Often the general form of both θ_k and u_{ij} are derived by some appropriate theory and then used in connection with some free variational parameters to be optimized.

Let us discuss first the appropriate form of the "pseudopotential" for Coulomb systems. There are important analytical properties for the "pseudopotential" that can be easily derived. Consider bringing two particles together and let us examine the dominant terms in the local energy. In a good trial action, the singularities in the kinetic energy must compensate those in the potential energy. The local energy for the two particle system is

$$e_L(r_{ij}) = e^{u_{ij}} \hat{h}_{ij}[e^{-u_{ij}}] = v_{ij}(r_{ij}) + \lambda_{ij}\left[\nabla^2 u_{ij} - (\nabla u_{ij})^2\right] \tag{50}$$

where $\lambda_{ij} = \lambda_i + \lambda_j$, $\hat{h}_{ij}$ is the two body hamiltonian with the interaction potential v_{ij} and the trial wave function $\exp[-u_{ij}]$. Spin symmetry has been disregarded as well as the trivial term related to the center of mass motion. Therefore the short distance behavior of any good form of the pseudopotential should follow the solution of the two body Schrödinger equation. For the Coulomb potential the "cusp" condition derives from this constraint. Indeed substituting $v_{ij} = e^2 z_i z_j / r$ in (50) and zeroing the coefficient of the dominant power of r for $r \to 0$ provides

$$\left.\frac{du_{ij}}{dr}\right|_0 = -\frac{e^2 z_i z_j}{\lambda_{ij}(D-1)} \tag{51}$$

It is also important to reproduce the correct behavior at large distances where a description in terms of collective coordinates is appropriate. The

long-wavelength modes are important for the low energy response properties and are also the slowest modes to converge in QMC. It is possible to show that, within the Random Phase Approximation (RPA), the local energy is minimized by imposing

$$u_k^{ee} = -\frac{1}{2} + \sqrt{1 + a_k} \tag{52}$$

$$u_k^{ep} = \frac{-a_k}{\sqrt{1 + a_k}} \tag{53}$$

with $a_k = 12r_s/k^4$ and the electron sphere radius r_s is related to the volume per electron by $v = 4\pi r_s^3/3$ in atomic units [32]. Here $u_k^{\alpha\beta}$ indicates the Fourier Transform of $u_{\alpha\beta}(r)$. The obtained form of the "pseudopotential" is correct at short and long distances but not necessarily in between because of the approximation. One can improve slightly the quality of the VMC results considering the form

$$\tilde{u}_{ij}(r) = u_{ij}^{RPA}(r) - \alpha_{ij} e^{-r^2/w_{ij}^2} \tag{54}$$

with the variational parameter α_{ij}, w_{ij}. The additional term preserves the short and long distance behavior of the RPA function. This form of the pair trial function introduces four variational parameters, namely $\alpha_{ee}, w_{ee}, \alpha_{ep}, w_{ep}$.

We discuss now the choice of the spin orbitals. The spin-orbitals are conceptually more important than the pseudopotential because they provide the nodal structure of the trial function. With the fixed node approximation in RQMC, the projected ground state has the same nodal surfaces of the trial function, while the other details of the trial function are automatically "optimized" for increasing projection time. It is thus important that the nodes provided by given spin-orbitals be accurate. Moreover, the optimization of nodal parameters (see below) is, in general, more difficult and unstable than for the pseudopotential parameters [6].

The simplest form of spin-orbitals for a system with translational invariance are plane waves (PW) $\theta_{\boldsymbol{k}}(\boldsymbol{r}, \sigma) = \exp[\imath \boldsymbol{k} \cdot \boldsymbol{r}]$. This form was used in the first QMC study of metallic hydrogen [33]. It is particularly appealing for its simplicity and still qualitatively correct since electron-electron and electron-proton correlations are considered through the "pseudopotential". The plane waves orbitals are expected to reasonably describe the nodal structure for metallic atomic hydrogen, but no information about the presence of protons appears in the nodes with PW orbitals.

For insulating molecular hydrogen (i.e for $r_s \geq 1.5$), it is preferred to use localized gaussian orbitals. There are different possibilities: a single isotropic gaussian centered at the middle of the bond was used in the first QMC study [33], while a single multivariate gaussian was used in the first CEIMC attempt [15, 16]. Another possibility is to form a molecular orbitals as linear combination of two atomic gaussian orbitals centered on each proton:

$$\theta_k(\boldsymbol{r}, \boldsymbol{s}_{k,1}, \boldsymbol{s}_{k,2}) = \exp(-c|\boldsymbol{r} - \boldsymbol{s}_{k,1}|^2) + \exp(-c|\boldsymbol{r} - \boldsymbol{s}_{k,2}|^2) \tag{55}$$

where $\boldsymbol{s}_{k,j}$ is the position of the j^{th} proton of the k^{th} molecule. This kind of orbitals have a single variational parameter c. At present we are experimenting using a trial molecular wave function with these orbitals multiplied by the corrected RPA Jastrow within the CEIMC.

The trouble with this strategy is that one should know which phase is stable before performing the calculation. This is typical of ground state studies. However in CEIMC we would rather let the system find its own state for given temperature and density (or pressure). In particular, this approach is not appropriate to address the interesting region of molecular dissociation and metallization. This problem can be solved by using orbitals obtained as solution of a single-electron problem as in band structure calculations or in self-consistent mean field methods. In previous works on ground state hydrogen, the single electron orbitals for a given protonic state S, were obtained from a DFT-LDA calculation [34–36]. One of this study [35] established that energies from plane-waves determinants in metallic hydrogen are higher than the more accurate estimates from DFT-LDA orbitals by 0.05 eV/atom at the density at which the transition between molecular and metallic hydrogen is expected ($r_s = 1.31$). Obtaining the orbitals from a DFT-LDA calculation has, however, several drawbacks in connection with the CEIMC. While for protons on a lattice we can solve the self-consistent theory for a primitive cell only, in a disordered configuration, we need to consider the entire simulation box. This is very expensive in CPU time and memory for large systems. Moreover, combining the LDA orbitals with Jastrow to improve the accuracy is not straightforward; substantial modification of the orbitals might be necessary requiring a reoptimization of the orbitals and the correlation factors, in principle, at each new ionic position.

Beyond the Pair Product Trial Function

Over the years there have been important progress in finding trial functions substantially more accurate then the pair product form for homogeneous systems [12,13]. Within the generalized Feynman-Kac formalism, it is possible to systematically improve a given trial function [13, 14]. The first corrections to the pair product action with plane wave orbitals are a three-body correlation term which modifies the correlation part of the trial function (Jastrow) and a "backflow" transformation which changes the orbitals and therefore the nodal structure (or the phase) of the trial function [14]. The new trial function has the form

$$\Psi_T(R, \Sigma|S) = det[\theta_k(\boldsymbol{x}_i, \sigma_i|S)]e^{-U_2-U_3} \tag{56}$$

where $U_2 = \sum_{i<j} \tilde{u}_{ij}$ is the two body "pseudopotential" discussed before, U_3 the three-body term of the form

$$U_3 = -\sum_{i=1}^{N_e} \left[\sum_{j=1}^{N} \xi_{ij}(r_{ij}) \boldsymbol{r}_{ij} \right]^2 \tag{57}$$

and finally the "quasiparticle" coordinates appearing in the plane wave orbitals are given by

$$\boldsymbol{x}_i = \boldsymbol{r}_i + \sum_{j=1}^{N} \eta_{ij}(r_{ij})\boldsymbol{r}_{ij}; \qquad (i = 1, \ldots, N_e) \tag{58}$$

The functional form of the three-body term is that of a squared two-body force so its evaluation is not slower than a genuine 2-body term. In the homogeneous electron system, this term is particularly relevant at low density where correlation effects are dominant. On the other hand, the backflow transformation is more relevant at high density because in this limit the fermionic character of the system dominates. The same general framework should hold for hydrogen although a throughout study of the relative importance of those effects with density is still missing. The fundamental improvement of backflow orbitals for metallic hydrogen is that the nodal structure of the wave functions depends now on the proton positions. This provides better total energies for static protonic configurations [14] and improved energy differences and liquid structure in CEIMC [16,37]. However it is not clear how appropriate this kind of wave function will be when entering in the molecular phase of hydrogen.

The unknown functions, $\xi_{ij}(r), \eta_{ij}(r)$ in (57) and (58) need to be parameterized in some way. In a first attempt we have chosen gaussians with variance and amplitude as new variational parameters [16]. This form was shown to be suitable for homogeneous electron gas [13]. Approximate analytical forms for $\xi_{ij}(r)$ and $\eta_{ij}(r)$, as well as for the two-body pseudopotential, have been obtained later in the framework of the Bohm-Pines collective coordinates approach [14]. This form is particularly suitable for the CEIMC because there are no parameters to be optimized. This trial function is faster than the pair product trial function with the LDA orbitals, has no problems when protons move around and its nodal structure has the same quality as the corresponding one for the LDA Slater determinant [14]. We have extensively used this form of the trial wave function for CEIMC calculations of metallic atomic hydrogen.

Trial Function Optimization

For metallic hydrogen we have described a parameter-free trial function which does not need optimization. However, if we use the pair proton action both for molecular or LDA orbitals, we are left with free parameters in the Jastrow factor and with the width of the gaussians for molecular orbitals. Optimization of the parameters in a trial function is crucial for the success of VMC. Bad upper bounds do not give much physical information. Good trial functions will be needed in the Projector Monte Carlo method. First, we must decide on what to optimize and then how to perform the optimization. There are several possibilities for the quantity to optimize and depending on the physical system, one or other of the criteria may be best.

- The variational energy: E_V. If the object of the calculation is to find the least upper bound one should minimize E_V. There is a general argument suggesting that the trial function with the lowest variational energy will maximize the efficiency of Projector Monte Carlo [38].
- The variance of the local energy: $\sigma^2 = \int |\mathcal{H}\Psi|^2 - E_V^2$. If we assume that every step on a QMC calculation is statistically uncorrelated with the others, then the variance of the average energy will equal σ^2/p where p is the number of steps. The minimization of σ^2 is statistically more robust than the variational energy because it is a positive definite quantity with zero as minimum value. One can also minimize a linear combination of the variance and the variational energy.
- The overlap with the exact wave function: $\int \Psi\phi$. If we maximize the overlap, we find the trial function closest to the exact wave function in the least squares sense. This is the preferred quantity to optimize if you want to calculate correlation functions, not just ground state energies since, then, the VMC correlation functions will be closest to the true correlation functions. Optimization of the overlap will involve a Projector Monte Carlo calculation to determine the change of the overlap with respect to the trial function so it is more complicated and rarely used.

The most direct optimization method consists of running independent VMC calculations using different set of numerical values for the variational parameters. One can fit the energies to a polynomial, performing more calculations near the predicted minimum and iterating until convergence in parameter space is attained. The difficulty with this direct approach is that close to the minimum, the independent statistical errors will mask the variation with respect to the trial function parameters. This is because the derivative of the energy with respect to trial function parameters is very poorly calculated. Also, it is difficult to optimize, in this way, functions involving more than 3 variational parameters because so many independent runs are needed to cover the parameter space.

A correlated sampling method, known as reweighting [39,40] is much more efficient. One samples a set of configurations $\{R_j\}$ (usually several thousand points at least) according to some distribution function, usually taken to be the square of the wavefunction for some initial trial function: $|\Psi_T(R;\{\alpha\}_0)|^2$. Then, the variational energy (or the variance) for trial function nearby in parameter space can be calculated by using the same set of points:

$$E_v(a) = \frac{\sum_j w(R_j,\{\alpha\})E_L(R_j,\{\alpha\})}{\sum_j w(R_j,\{\alpha\})}, \tag{59}$$

where the weight factor, $w(R) = |\Psi_T(R;\{\alpha\})/\Psi_T(R;\{\alpha\}_0)|^2$, takes into account that the distribution function changes as the variational parameters change. One then can use a minimizer to find the lowest variational energy or variance as a function of $\{\alpha\}$ keeping the configurations fixed. However, there is an instability: if the parameters move too far away, the weights span too

large of a range and the error bars of the energy become large. The number of effective points of a weighted sum is:

$$N_{eff} = \left(\sum w_j\right)^2 / \sum w_j^2. \tag{60}$$

If this becomes much smaller than the number of points, one must resample and generate some new points. When minimizing the variance, one can also simply neglect the weight factors. Using the reweighting method one can find the optimal value of wavefunction containing tens of parameters.

2.5 Twist Average Boundary Conditions

Almost all QMC calculations in periodic boundary conditions have assumed that the phase of the wave function returns to the same value if a particle goes around the periodic boundaries and returns to its original position. However, with these boundary conditions, delocalized fermion systems converge slowly to the thermodynamic limit because of shell effects in the filling of single particle states. Indeed, with periodic boundary conditions the Fermi surface of a metal will be reduced to a discrete set of points in k-space. The number of k-points is equal to the number of electrons of same spin and therefore it is quite limited.

One can allow particles to pick up a phase when they wrap around the periodic boundaries,

$$\Psi_{\boldsymbol{\theta}}(\boldsymbol{r}_1 + L\boldsymbol{n}, \boldsymbol{r}_2, \cdots) = e^{i\boldsymbol{\theta}}\Psi_{\boldsymbol{\theta}}(\boldsymbol{r}_1, \boldsymbol{r}_2, \ldots)\,. \tag{61}$$

where we have assumed a cubic box of size L and $\boldsymbol{n}$ is a vector of integers. The boundary condition $\boldsymbol{\theta} = 0$ is periodic boundary conditions (PBC), and the general condition with $\boldsymbol{\theta} \neq 0$, twisted boundary conditions (TBC). If the periodic boundaries are used in all directions, each dimension can have an independent twist. Hence, in three dimension (3D), the twist angle is a three components vector. The free energy and therefore all equilibrium properties are periodic in the twist: $F(\boldsymbol{\theta} + 2\pi\boldsymbol{n}) = F(\boldsymbol{\theta})$ so that each component of the twist can be restricted to be in the range $-\pi < \theta_i \leq \pi$.

The use of twisted boundary conditions is commonplace for the solution of the band structure problem for a periodic solid, particularly for metals. In order to calculate properties of an infinite periodic solid, properties must be averaged by integrating over the first Brillouin zone.

For a degenerate Fermi liquid, finite-size shell effects are much reduced if the twist angle is averaged over: twist averaged boundary conditions (TABC) [30]. For any given property $\hat{A}$ the TABC is defined as

$$\langle\, \hat{A} \,\rangle = \int_{-\pi}^{\pi} \frac{d\boldsymbol{\theta}}{(2\pi)^d} \,\langle\, \Psi_{\boldsymbol{\theta}} | \hat{A} | \Psi_{\boldsymbol{\theta}} \,\rangle \tag{62}$$

TABC is particularly important in computing properties that are sensitive to the single particle energies such as the kinetic energy and the magnetic susceptibility. By reducing shell effects, accurate estimations of the thermodynamic limit for these properties can be obtained already with a limited number of electrons. What makes this very important is that the most accurate quantum methods have computational demands which increase rapidly with the number of fermions. Examples of such methods are exact diagonalization (exponential increase in CPU time with N), variational Monte Carlo (VMC) with wave functions having backflow and three-body terms [13] (increases as N^4), and transient-estimate and released-node Diffusion Monte Carlo methods [41] (exponential increase with N). Moreover, size extrapolation is impractical within CEIMC since it would have to be performed for any proposed ionic move prior to the acceptance test. Methods which can extrapolate more rapidly to the thermodynamic limit are crucial in obtaining high accuracy.

Twist averaging is especially advantageous in combination with stochastic methods (i.e. QMC) because the twist averaging does not necessarily slow down the evaluation of averages, except for the necessity of doing complex rather than real arithmetic. In a metallic system, such as hydrogen at very high pressure, results in the thermodynamic limit require careful integration near the Fermi surface because the occupation of states becomes discontinuous. Within LDA this requires "k–point" integration, which slows down the calculation linearly in the number of k-points required. Within QMC such k-point integration takes the form of an average over the (phase) twist of the boundary condition and can be done in parallel with the average over electronic configurations without significantly adding to the computational effort.

In CEIMC we can take advantage of the twist averaging to reduce the noise in the energy difference for the acceptance test of the penalty method (see below). In the electron gas, typically 1000 different twist angles are required to achieve convergence [30]. We have used the same number of twist angles in CEIMC calculations of metallic hydrogen. Different strategies can be used to implement the TABC [30]. We have used a fixed 3D grid in the twist angle space, at each grid point run independent QMC calculations and then averaged the resulting properties. This procedure can be easily and efficiently implemented on a parallel computer. Recently, we have devised a sampling procedure to randomize the grid points at each ionic step. We have limited experience, but, so far, we have evidence that good convergence in the electronic and ionic properties can already be reached for a number of twist angles as low as 30 [42].

2.6 Sampling Electronic States: The "Bounce" Algorithm

In this section we describe the way we have implemented electronic move in the CEIMC method. In particular we present an original algorithm for RQMC, particularly suitable for CEIMC, called the "bounce" algorithm.

First, how do the particles move in VMC? In the continuum it is usually more efficient to move the particles one at a time by adding a random vector to a particle's coordinate, where the vector is either uniform inside of a cube, or is a normally distributed random vector centered around the old position. Unfortunately, this procedure cannot be used with backflow orbitals. This is because the backflow transformation couples all the electronic coordinates in the orbitals so that once a single electron move is attempted the entire Slater determinant needs to be recomputed, an $O(N^3)$ operation. It is much more efficient to move all electrons at once, although global moves could become inefficient for large systems.

Next we describe the electronic sampling within RQMC. In the original work on RQMC [18], the electronic path space was sampled by a simple reptation algorithm, an algorithm introduced to sample the configurational space of linear polymer chains [43]. Remember that in RQMC the electronic configurational space is the space of $3N_e$-dimensional random paths of length "t". In practice, the imaginary time is discretized in M time slices $\tau = t/M$ and the paths become discrete linear chains of $M+1$ beads. Let us indicate with Q the entire set of $3N(M+1)$ coordinates $Q = \{R_0, \ldots, R_M\}$. According to (33), (34) and (36), the path distribution is

$$\Pi(Q) = |\Psi_T(R_0)\Psi_T(R_M)| e^{-\sum_{k=1}^{M} L_s(R_{k-1},R_k,\tau)} \\ e^{-\tau\left[\frac{E_L(R_0)}{2}+\sum_{k=1}^{M-1} E_L(R_k)+\frac{E_L(R_M)}{2}\right]} \tag{63}$$

Given a path configuration Q, a move is done in two stages. First one of the two ends (either R_0 or R_M) is sampled with probability 1/2 to be the growth end R_g. Then a new point near the growth end is sampled from a Gaussian distribution with center at $R_g + 2\lambda\tau F(R_g)$. In order to keep the number of links on the path constant, the old tail position is discarded in the trial move. The move is accepted or rejected with the Metropolis formula based on the probability of a reverse move. For use in the following, let us define the direction variable d as $d = +1$ for a head move ($R_g = R_M$), and $d = -1$ for a tail move ($R_g = R_0$). In standard reptation, the direction d is chosen randomly at each attempted step. The transition probability $P(Q \to Q')$ is the product of an attempt probability $T_d(Q \to Q')$ and an acceptance probability $a_d(Q \to Q')$. The paths distribution $\Pi(Q)$ does not depend on the direction d in which it was constructed. In the Metropolis algorithm, the acceptance probability for the attempted move is

$$a_d(Q \to Q') = \min\left[1, \frac{\Pi(Q')T_{-d}(Q' \to Q)}{\Pi(Q)T_d(Q \to Q')}\right] \tag{64}$$

which ensures that the transition probability $P_d(Q \to Q')$ satisfies detailed balance

$$\Pi(Q)P_d(Q \to Q') = \Pi(Q')P_{-d}(Q' \to Q) \tag{65}$$

The autocorrelation time of this algorithm, that is the number of MC steps between two uncorrelated configurations, scales as $[M^2/A]$, where A is

the acceptance rate of path moves, an unfavorable scaling for large M (i.e. large projection time t). Moreover the occasional appearance of persistent configurations bouncing back and forth without really sampling the configuration space has been previously observed [44]. These are two very unfavorable features, particularly in CEIMC, where we need to perform many different electronic calculations. There is a premium for a reliable, efficient and robust algorithm.

We have found that a minimal modification of the reptation algorithm solves both of these problems. The idea is to chose randomly the growth direction at the beginning of the Markov chain, and reverse the direction upon rejection only, the "bounce" algorithm.

What follows is the proof that the bounce algorithm samples the correct probability distribution $\Pi(Q)$. The variable d is no longer randomly sampled, but, as before, the appropriate move is sampled from the same Gaussian distribution $T_d(Q \to Q')$ and accepted according to the (64). In order to use the techniques of Markov chains, we need to enlarge the state space with the direction variable d. In the enlarged configuration space $\{Q, d\}$, let us define the transition probability $P(Q, d \to Q', d')$ of the Markov chain. The algorithm is a Markov process in the extended path space, and assuming it is ergodic, it must converge to a unique stationary state, $\Upsilon(Q, d)$ satisfying the eigenvalue equation:

$$\sum_{Q,d} \Upsilon(Q, d)\, P(Q, d \to Q', d') = \Upsilon(Q', d') \; . \tag{66}$$

We show that our desired probability $\Pi(Q)$ is solution of this equation. Within the imposed rule, not all transitions are allowed, but $P(Q, d \to Q', d') \neq 0$ for $d = d'$ and $Q \neq Q'$ (accepted move), or $d' = -d$ and $Q = Q'$ (rejected move) only. Without loss of generality let us assume $d' = +1$ since we have symmetry between ± 1. Equation (66) with $\Upsilon(Q, d)$ replaced by $\Pi(Q)$ is

$$\Pi(Q')P(Q', -1 \to Q', 1) + \sum_{Q \neq Q'} \Pi(Q)P(Q, 1 \to Q', 1) = \Pi(Q') \; . \tag{67}$$

Because of detailed balance (65), we have

$$\Pi(Q)P(Q, 1 \to Q', 1) = \Pi(Q')P(Q', -1 \to Q, -1)$$

which, when substituted in this equation gives

$$\Pi(Q') \left[P(Q', -1 \to Q', 1) + \sum_{Q} P(Q', -1 \to Q, -1) \right] = \Pi(Q') \; . \tag{68}$$

Note that we have completed the sum over Q with the term $Q = Q'$ because its probability vanishes. The term in the bracket exhausts all possibilities for a move from the state $(Q', -1)$, thus it adds to one. Hence $\Pi(Q)$ is a solution of (66) and by the theory of Markov chains, it is the probability distribution of the stationary state.

3 Sampling Ionic States: The Penalty Method

In Metropolis Monte Carlo a Markov chain of ionic states S is generated according to the Boltzmann distribution $P(S) \propto e^{-\beta E_{BO}(S)}$ where $E_{BO}(S)$ is the Born-Oppenheimer energy for the ionic configuration S, and β the inverse temperature. From the state S a trial state S' is proposed with probability $T(S \to S')$ and the detailed balance condition is imposed by accepting the move with probability

$$A(S \to S') = \min \left[1, \frac{T(S' \to S) e^{-\beta E_{BO}(S')}}{T(S \to S') e^{-\beta E_{BO}(S)}} \right] \tag{69}$$

Under quite general conditions on the system and on the a-priori transition probability $T(S \to S')$, after a finite number of MC steps the Markov chain so generated will visit the states of the configurational space with a frequency proportional to their Boltzmann's weight [43].

In CEIMC estimate of $E_{BO}(S)$ is affected by statistical noise. If we ignore the presence of noise and we use the standard Metropolis algorithm, the results will be biased, the amount of bias increasing for increasing noise level. A possible solution would be to run very long QMC calculations in order to get a negligibly small noise level resulting in a negligible bias. However, the noise level decreases as the number of independent samples to the power 1/2, that is to decrease the noise level by one order of magnitude we should run 100 times longer, an unfavorable scaling if we realize that we have to repeat such calculation for any attempted move of the ions. The less obvious but far more efficient solution is to generalize the Metropolis algorithm to noisy energies. This is done by the Penalty Method [45]. The idea is to require the detailed balance to hold on average and not for any single energy calculation.

Let us consider two ionic states (S, S') and call $\delta(S, S')$ the "instantaneous" energy difference times the inverse temperature. Let us further assume that the average and the variance of $\delta(S, S')$ over the noise distribution $P(\delta | S \to S')$ exhist

$$\Delta(S, S') = \beta] E_{BO}(S') - E_{BO}(S)] = \langle\, \delta(S, S') \,\rangle \tag{70}$$

$$\sigma^2(S, S') = \langle\, (\delta(S, S') - \Delta(S, S'))^2 \,\rangle \tag{71}$$

We introduce the "instantaneous" acceptance probability, $a(\delta | S, S')$ and impose the detailed balance to hold for the average of $a(\delta | S, S')$ over the distribution of the noise

$$A(S \to S') = e^{-\Gamma(S,S')} A(S' \to S) \tag{72}$$

where

$$A(S \to S') = \int_{-\infty}^{\infty} d\delta P(\delta | S \to S') a(\delta | S, S') \tag{73}$$

and we have defined

$$\Gamma(S,S') = \Delta(S,S') - \ln\left[\frac{T(S'\to S)}{T(S\to S')}\right] \tag{74}$$

If we assume the quite general conditions $a(\delta|S,S') = a(\delta)$ and $P(\delta|S \to S') = P(-\delta|S' \to S)$ to hold, the detailed balance can be written

$$\int_{-\infty}^{\infty} d\delta P(\delta|S\to S')\left[a(\delta) - e^{-\Gamma}a(-\delta)\right] = 0 \tag{75}$$

which, supplemented by the condition $a(\delta) \geq 0$, is the equation to solve in order to obtain the acceptance probability $a(\delta)$. The difficulty is that during the MC calculation we do not know either $P(\delta|S \to S')$ nor $\Delta(S,S')$.

In order to make progress let us assume, as it happens in many interesting cases, that the noise of the energy difference is normally distributed so that

$$P(\delta|S\to S') = (2\pi\sigma^2)^{-1/2}\exp\left[-(\delta-\Delta)^2/2\sigma^2\right] \tag{76}$$

Let us, moreover, assume that we know the value of the variance σ. It is not difficult to check that the solution of (75) is

$$a_n(\delta|\sigma) = \min\left[1, \frac{T(S'\to S)}{T(S\to S')}\exp\left(-\delta - \frac{\sigma^2}{2}\right)\right] \tag{77}$$

The uncertainty in the energy difference just causes a reduction in the acceptance probability by an amount $\exp(-\sigma^2/2)$ for $\delta > -\sigma^2/2$. The integral of $a_n(\delta|\sigma)$ over the guassian measure provides

$$\begin{aligned} A(S\to S') = {} & \tfrac{1}{2}\,\mathrm{erfc}\left\{\left[\sigma^2/2 + \Gamma(S\to S')\right]/(\sqrt{2}\sigma)\right\} + \\ & \tfrac{1}{2}\,\mathrm{erfc}\left\{\left[\sigma^2/2 - \Gamma(S\to S')\right]/(\sqrt{2}\sigma)\right\} e^{-\Gamma(S\to S')} \end{aligned} \tag{78}$$

which satisfies (72) since $\Gamma(S' \to S) = -\Gamma(S \to S')$. Note that (77) reduces to the standard Metropolis form for vanishing σ [43].

An important issue is to verify that the energy differences are normally distributed. Recall that if the moments of the energy difference are bounded, the central limit theorem implies that given enough samples, the distribution of the mean value will be Gaussian. Careful attention to the trial function to ensure that the local energies are well behaved may be needed.

In practice not only the energy difference Δ but also the variance σ is unknown and must be estimated from the data. Let us assume that, for a given pair of ionic states (S, S'), we generate n statistically uncorrelated estimates of the energy difference $\{y_1, \ldots, y_n\}$ each normally distributed with their first and second moments defined in the usual way

$$\Delta = \langle\, y_i \,\rangle \tag{79}$$

$$\sigma^2 = \langle\, (y_i - \Delta)^2 \,\rangle \tag{80}$$

Unbiased estimates of Δ and σ^2 are

$$\delta = \frac{1}{n}\sum_{i=1}^{n} y_i \tag{81}$$

$$\chi^2 = \frac{1}{n(n-1)}\sum_{i=1}^{n}(y_i - \delta)^2 \tag{82}$$

An extension of the derivation above provides [45]

$$a(\delta, \chi^2, n) = \min\left[1, \frac{T(S' \to S)}{T(S \to S')}\exp(-\delta - u_B)\right] \tag{83}$$

where

$$u_B = \frac{\chi^2}{2} + \frac{\chi^4}{4(n+1)} + \frac{\chi^6}{3(n+1)(n+3)} + \cdots \tag{84}$$

The first term in the r.h.s. of eq. (84) is the penalty in the case we know the variance. The error of the noise causes extra penalty which decreases as the number of independent samples n grows. In the limit of large n the first term dominates and we recover (77). Equation (84) must be supplemented by the condition $\chi^2/n \leq 1/4$ for the asymptotic expansion (84) to converge and the instantaneous acceptance probability to be positive [45].

The noise level of a system can be characterized by the relative noise parameter, $f = (\beta\sigma)^2 t/t_0$, where t is the computer time spent reducing the noise, and t_0 is the computer time spent on other pursuits, such as optimizing the VMC wave function or equilibrating the RQMC runs. A small f means little time is being spent on reducing noise, where a large f means much time is being spent reducing noise. For a double well potential, the noise level that gives the maximum efficiency is around $\beta\sigma \approx 1$, with the optimal noise level increasing as the relative noise parameter increases [45]. In CEIMC runs for hydrogen the noise level $\beta\sigma$ ranges between 0.3 and 3, the optimal value being around 1.

3.1 Efficient Strategies for Electronic Energy Differences

As explained above, we need to evaluate the energy difference and the noise between two protonic configurations (S, S'). The distance in configurational space between S and S' in an attempted move is however quite limited since we have to move all protons at once. Indeed, each backflow orbital depends on the position of all protons and single proton moves would require recomputing the entire determinant for each attempted move, a $\mathrm{O}(N^4)$ operations for a global move. Instead, moving all protons together requires a single determinant calculation per ionic move, a $\mathrm{O}(N^3)$ operation. In this case, performing two independent electronic calculations for S and S' to estimate the energy difference would be very inefficient since $\Delta E_{BO} \ll E_{BO}(S)$ and the noise

on the energy difference would just be twice the noise on the single energy estimate. The strategy to adopt is to compute the energy difference from correlated sampling, i.e. sampling the electronic configurational space from a distribution which depends both on S and S' and estimating the energy difference and the other electronic properties of interest by reweighting the averages [16]. It is possible to show that the optimal sampling function, i.e. the sampling distribution for which the variance of the energy difference is minimal, takes the form

$$P(Q|S,S') \propto |\Pi(Q|S)(E_{BO}(S) - \langle E_{BO}(S)\rangle) - \Pi(Q|S')(E_{BO}(S') - \langle E_{BO}(S')\rangle)| \tag{85}$$

where $\langle\, E_{BO}\,\rangle$ is the estimate of the BO energy. In order to use this sampling probability we need to estimate the BO energies of the two states before performing the sampling. A simpler form which avoid this problem is

$$P(Q|S,S') \propto \Pi(Q|S) + \Pi(Q|S') \tag{86}$$

We emphasize that the "reptile" space for the electron paths depends on the proton coordinates so that, because of the fixed-node restriction for fermions, legal paths for S may or may not be legal for S' and vice-versa. These two forms of importance sampling have the property that they sample regions of both configuration spaces (S and S') and make the energy difference rigorously correct with a bounded variance.

3.2 Pre-Rejection

We can use multi-level sampling to make CEIMC more efficient [19]. An empirical potential is used to "pre-reject" moves that would cause particles to overlap and be rejected anyway. A trial move is proposed and accepted or rejected based on a classical potential

$$A_1 = \min\left[1, \frac{T(S \to S')}{T(S' \to S)} \exp(-\beta \Delta V_{cl})\right] \tag{87}$$

where $\Delta V_{cl} = V_{cl}(S') - V_{cl}(S)$ and T is the sampling probability for a move. If it is accepted at this first level, the QMC energy difference is computed and accepted with probability

$$A_2 = \min\left[1, \exp(-\beta \Delta E_{BO} - u_B) \exp(\beta \Delta V_{cl})\right] \tag{88}$$

where u_B is the noise penalty. Compared to the cost of evaluating the QMC energy difference, computing the classical energy difference is much less expensive. Reducing the number of QMC energy difference evaluations reduces the overall computer time required.

For metallic hydrogen a single Yukawa potential was always found to be suitable for pre-rejection. For molecular hydrogen we use instead a Silvera-Goldman potential [46] riparametrized in such a way to have the center of interaction on any single proton in the molecule rather than on the molecular center of mass. In practice, we take a single Yukawa potential for intermolecular proton-proton interaction and the Kolos-Wolniewski potential [47] for the bonding interaction. The Yukawa screening length and the prefactor are optimized to reproduce the results of the Silvera-Goldman model. This new potential is suitable for pre-rejecting all types of moves that we attempt in the molecular hydrogen, namely molecular rotations, bond stretching and molecular translations. The original Silvera-Goldmann potential being spherically symmetric around the molecular center is not suitable to pre-reject the rotational moves.

4 Quantum Protons

By increasing pressure and/or decreasing temperature, ionic quantum effects can become relevant. Those effects are important for hydrogen at high pressure [7, 48]. Static properties of quantum systems at finite temperature can be obtained with the Path Integral Monte Carlo method (PIMC) [19]. We need to consider the ionic thermal density matrix rather than the classical Boltzmann distribution:

$$\rho_p(S, S'|\beta) = \langle\, S|e^{-\beta(\hat{K}_p+\hat{E}_{BO})}|S'\,\rangle \tag{89}$$

where $\hat{K}_p$ is the ionic kinetic energy operator and $\beta = (K_B T)^{-1}$ is the inverse physical temperature. Thermal averages of ionic operators $\hat{A}_p$ (diagonal in configurational space) are obtained as

$$A_p(\beta) = \frac{1}{Z(\beta)} \int dS A_p(S) \rho_p(S, S|\beta) \tag{90}$$

where Z is the partition function

$$Z(\beta) = \int dS \rho_p(S, S|\beta) = e^{-\beta F} \tag{91}$$

and F is the Helmholtz free energy of the system. As before, the thermal density matrix can be computed by a factorization of β in many (P) small intervals (time slices $\tau_p = \beta/P$) and by a suitable approximation for the "high temperature" (or short time) density matrix. According to the Feynman-Kac formula (see (24) and (35)) the diagonal part of the thermal density matrix is the sum over all closed paths, i.e. paths starting at S and returning to S after a "time" β. This is the famous "isomorphism" between quantum particles and ring polymers [19,21]. Considering particle statistics in the PIMC is more difficult than in RQMC. The reason is that in PIMC the state of the classical

system, which has no symmetry built in, plays the role of the trial functions in RQMC and permutations need to be sampled explicitly with an additional level of difficulty in the method [19, 26]. However, protonic statistics become relevant when the quantum dispersion is comparable to the interionic distances $\Lambda_p = \sqrt{2\lambda_p\beta} \approx (N_p/V)^{-1/3} = n_p^{-1/3}$. This define a degeneracy temperature $k_B T_D(n_p) = 2\lambda_p n_p^{2/3}$ below which quantum statistics need to be considered. For hydrogen $T_D \simeq 66.2(K)/r_s^2$, where r_s is the usual ion sphere radius of coulomb systems $r_s = (3/4\pi n_p)^{1/3}$. Therefore proton statistics in metallic hydrogen ($r_s \leq 1.3$) becomes relevant below 50K depending on the density, a regime that we have not investigated yet. Proton statistics in molecular hydrogen is also quite important and results in the separation between ortho- and para-hydrogen [49]. Because this effect is relevant only at low temperature, we have disregarded it as well.

In order to implement the PIMC we need a suitable approximation for the high temperature density matrix $\rho_p(S, S'|\tau_p)$. We could use either the primitive approximation or the importance sampling approximation described earlier. However a better approximation, in particular for distinguishable particles, is the pair product action [19] which closely resembles the pair trial function. The idea is to build the many body density matrix as the product over all distinct pairs of a two-body density matrices obtained numerically for a pair of isolated particles. At high temperature the system approaches the classical Boltzmann distribution which is indeed of the pair product form. The method is described in detail in [19]. Here we just explain how we can take advantage of this methodology within the CEIMC scheme. In order to use the method of pair action, we need to have a pair potential between quantum particles. In CEIMC, however, the interaction among protons is provided by the many-body BO energy. Our strategy is to introduce an effective two-body potential between protons $\hat{V}_e$ and to recast the ionic density matrix as

$$\begin{aligned} \rho_{_P}(S, S'|\tau_p) &= \langle\, S|e^{-\tau_p[\hat{H}_e+(\hat{E}_{BO}-\hat{V}_e)]}|S'\,\rangle \\ &\approx \langle\, S|e^{-\tau_p\hat{H}_e}|S'\,\rangle\; e^{-\frac{\tau_p}{2}[E_{BO}(S)-V_e(S)]+[E_{BO}(S')-V_e(S')]} \end{aligned} \tag{92}$$

where $\hat{H}_e = \hat{K}_p + \hat{V}_e$ and the corrections from the effective potential to the true BO energy are treated at the level of the primitive approximation. We can compute numerically the matrix elements of the effective pair density matrix $\hat{\rho}_e^{(2)}(\tau_p)$ as explained in [19]. The effective N_p-body density matrix is approximated by

$$\langle S|e^{-\tau_p\hat{H}_e}|S'\rangle \approx \prod_{ij}^{N_p}\langle s_i, s_j|\hat{\rho}_e^{(2)}(\tau_p)|s_i', s_j'\rangle = \rho_0(S, S'|\tau_p)e^{-\sum_{ij} u_e(\boldsymbol{s}_{ij}, \boldsymbol{s}_{ij}'|\tau_p)} \tag{93}$$

where ρ_0 is the free particle density matrix and $u_e(\boldsymbol{s}_{ij}, \boldsymbol{s}_{ij}'|\tau_p)$ is the effective pair action. The explicit form for the partition function is then

$$Z(\beta) = \int dS_1 \dots dS_P \prod_{k=1}^{P} \exp\left\{ -\frac{(S_k - S_{k+1})^2}{4\lambda_p \tau_p} - \sum_{ij} u_e(\boldsymbol{s}_{ij}^k, \boldsymbol{s}_{ij}^{k+1} | \tau_p) \right\} \exp\left\{ -\tau_p \sum_{k=1}^{P} [E_{BO}(S_k) - V_e(S_k)] \right\} \quad (94)$$

with the boundary condition: $S_{P+1} = S_1$. As for the pre-rejection step in the proton moves, we have used different effective potentials according to the system under consideration. In metallic hydrogen (a plasma) we have used a smooth screened coulomb form and found that it provides a fast convergence in τ_p. Convergence can be assessed by monitoring the various terms in the estimator for the proton kinetic energy [19]. A good effective potential should provide uniform convergence of the various orders in τ_p. With this effective potential, we have found convergence to the continuum limit ($\tau_p \to 0$) for $1/\tau_p \geq 3000\,\mathrm{K}$ which allows to simulate systems at room temperature with only $M \approx 10$ proton slices for $r_s \geq 1$. In molecular hydrogen we need to consider the extra contribution of the bonding potential. We have used the Kolos-Wolniewicz bonding potential in connection with the same smooth screened coulomb potential for the non bonding interactions. Convergence with τ_p is observed in a similar range.

A very nice feature of ionic PIMC in CEIMC is that considering ionic paths rather then classical point particles does not add any computational cost to the method. Let us suppose we run classical ions with a given level of noise $(\beta\sigma_{cl})^2$. Consider now representing the ions by P time slices. To have a comparable extra-rejection due to the noise we need a noise level per slice given by: $(\tau_p\sigma_k)^2 \approx (\beta\sigma_{cl})^2/P$ which provides $\sigma_k^2 \approx P\sigma_{cl}^2$. We can allow a noise per time slice P times larger which means considering P times less independent estimates of the energy difference per slice. However we need to run P different calculations, one for each different time slice, so that the amount of computing for a fixed global noise level is the same as for classical ions. In practice, however, because our orbitals depend on all proton positions, we are forced to move the proton positions at given imaginary time all together with a local (in imaginary time) update scheme. It is well known that the autocorrelation time of schemes with local updates rapidly increases with the chain length and this is the ultimate bottleneck of our present algorithm [19]. It is therefore essential to adopt the best factorization in order to minimize the number of time slices P needed and therefore to maximize the efficiency of the method.

When using TABC with quantum ions, for any proton time slice we should, in principle, perform a separate evaluation of the BO energy difference averaged over all twist angles. Instead at each protonic step, we randomly assign a subset of twist phases at each time slice and we compute the energy difference for that phase only. The TABC is then performed by adding up all the contributions from the different time slices. We have checked in few cases that this simplified procedure does not give detectable biases in the averages.

In practice we move all slices of all protons at the same time by a simple random move in a box and we pre-reject the moves with the effective pair action.

5 Summary of Results on High Pressure Hydrogen

In this section we briefly summarize some of the CEIMC results we have obtained for high pressure hydrogen. Figure 1 shows what is known and what has been predicted about the hydrogen phase diagram in a wide range of pressures and temperatures. The rectangular region in the right upper corner is the region where R-PIMC method can make reliable predictions [50–52]. There have been many studies of the ground state of hydrogen ($T = 0$) including some QMC investigations [33–36]. They have predicted a metallization density corresponding at $r_s = 1.31$ accompanied by a transition from a molecular m-hcp structure to a diamond lattice of protons. At intermediate temperatures a number of ab-initio Molecular Dynamics studies have been performed in the molecular and in the metallic phases, both in the crystal and in the liquid state [53–57].

Metallic Hydrogen

We first focus on the metallic system for pressure beyond the molecular dissociation threshold. In this region, hydrogen is a system of protons and delocalized electrons. At low enough temperature the protons order in a crystalline lattice which melts upon increasing temperature. The low temperature stable structure as a function of density is still under debate. The most accurate ground state QMC calculation [35], indicates that hydrogen at the edge of molecular dissociation will order in a diamond structure, and upon increasing density will undergo various structural transformations ultimately transforming to the bcc structure. However, these prediction are extrapolated from a single calculation at $r_s = 1.31$ and temperature effects are absent. With CEIMC we have investigated the density range $r_s \in [0.8, 1.2]$ and the temperature range $T \in [300\,\mathrm{K}, 5000\,\mathrm{K}]$ across the melting transition of the proton lattice and up to the lower limit of applicability of RPIMC. We limited the study to systems of $N_p = 32$ and $N_p = 54$ which, for cubic simulation boxes, form fcc and bcc lattices, respectively. We have observed the melting and refreezing of the protons and made a qualitative location of the melting line versus the density [16, 17] as shown by the green contour lines in Fig. 1.

A number of interesting question about the convergence and the efficiency of the CEIMC algorithm need to be answered before starting a systematic study. An important one is: how large must the electronic projection time be in order to get convergence in the energy difference to the ground state value and therefore obtain unbiased sampling in CEIMC? In order to answer such a question we have selected a pair of protonic configuration (S, S') at

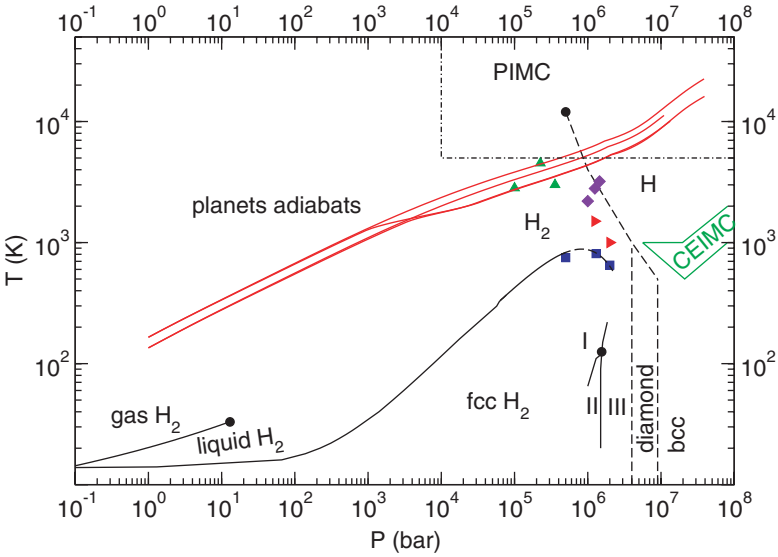

Fig. 1. Hydrogen phase diagram. Continuous transition lines are experimental results, *dashed lines* are theoretical prediction from various methods. *Squares* and *right-triangle* are ab-initio MD predictions of molecular melting [57] and molecular dissociation in the liquid phase [56]. The diamonds are shock-waves experimental data through the liquid metalization [58]. The *triangles* are earlier CEIMC data for the insulating molecular state [15, 16] while the light gray domain on the extreme right indicates the CEIMC prediction for the melting [17]. Dark gray lines are model adiabats for the interior of the giant planets of the solar system [59]

given density and computed the energy difference, together with total energy and variance, versus the electronic projection time. The results reported in Fig. 2 correspond to a system of $N_e = N_p = 16$ at $r_s = 1.31$ with the twist phase $\boldsymbol{\theta} = (0.4, 0.5, 0.6)\pi$. Results are obtained for an electronic time step $\tau_e = 0.02\,\mathrm{H}^{-1}$, a compromise between accuracy and efficiency. In panel a) we report the energy difference versus the projection time t to show that it does not depend on the projection time when using the accurate trial function with 3-body terms and backflow orbitals (3BF-A, black dots) discussed above. This suggests that the proton configuration space can be sampled using VMC for the electrons which is faster and more stable than RQMC. On the same panel we have reported the VMC estimate obtained with a trial function with a Slater determinant of simple plane waves and a two-body RPA Jastrow (SJ, red triangle) and a RQMC result obtained for a trial function with a 2-body RPA-Jastrow and a Slater determinant of self consistent LDA orbitals (LDA-J, blue squares). The simple SJ function at the variational level has a much larger energy difference (in absolute value) and therefore will provide a biased sampling of protonic configurations. It is not clear whether the RQMC projection with such trial function will recover the correct energy difference

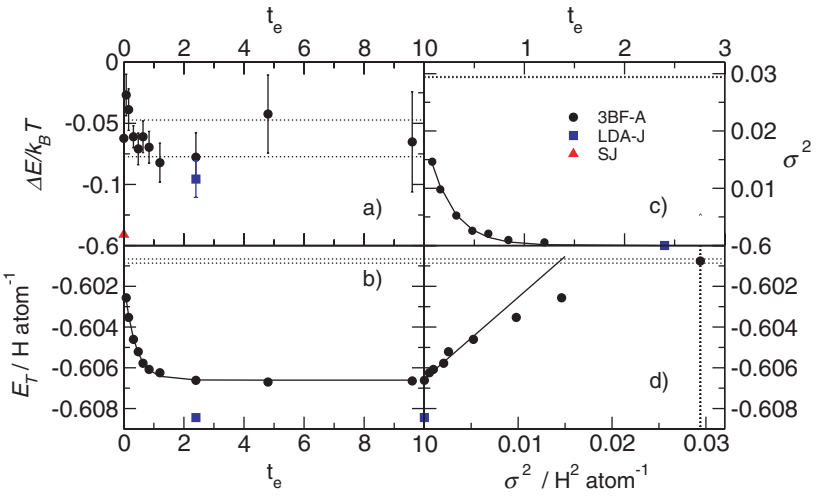

Fig. 2. $N_e = N_p = 16$, $r_s = 1.31$. Dependence of total energy, variance and energy difference for a pair of proton configurations (S, S') on the RQMC projection time. The study is performed for $\tau_e = 0.02\,\mathrm{H}^{-1}$. *Dotted lines* represent the variational estimates with their error bars. In panel **b**) and **c**) the lines are exponential fits to data and in panel **d**) the continuous line is a linear fit in the region $\sigma^2 \leq 0.005$. *Black circles* (3BF-A) are results obtained with the analitical three-body and backflow trial wave functions discussed earlier, the red triangle is a variational result with a Slater-Jastrow trial function with simple plane wave orbitals and the blue squares are results from a trial function with LDA orbitals and an optmized two-body Jastrow

(remember that the two kind of trial functions have different nodal structure). On the other hand, no difference is detected between the RQMC results from the 3BF-A and the LDA-J trial functions at the same projection time. This gives an indication of the quality of the 3BF-A nodal surfaces. The total energy and the variance of configuration S versus t are reported in panels b) and c), respectively. The two panels nicely illustrate the limiting process toward the fixed-node ground state operated by the projection (see (11)). Within the 3BF-A trial function we observe a large gain in energy with the projection time, the difference being $E(\infty) - E(0) = 5.7\,\mathrm{mH/at} = 1810\,\mathrm{K/at}$. In both panels the results of the SJ trial function are off scale, while we have reported the result of the LDA-J wave function. According to the total energy, the quality of LDA-J function is superior to the one of 3BF-A function for this configuration. The same quality was instead detected for the bcc lattice configuration [14]. Finally, in panel d) we report the total energy versus the variance of the 3BF-A trial function to show that both quantities go linearly with the error in the wave function when we are close enough to the ground state (the fixed-node one) [13].

In order to check that we can indeed sample the proton space with VMC energy differences, we have performed two test runs for the systems of $N_p =$

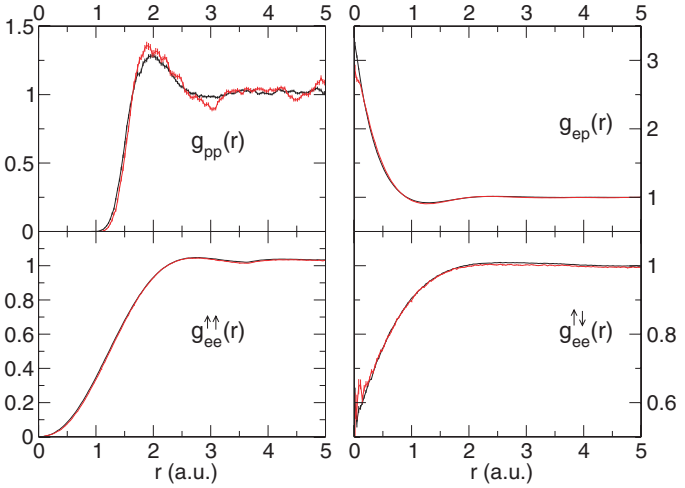

Fig. 3. $N_e = N_p = 54$, $r_s = 1.2$, $T = 5000\,\mathrm{K}$, Γ point. Comparison of VMC (*black*) and RQMC (*gray*) data for the pair correlation functions. The projection time in RQMC is $t_e = 0.68\,\mathrm{H}^{-1}$ with an electronic time step of $\tau_e = 0.01\,\mathrm{H}^{-1}$. Protons are considered as classical point particles

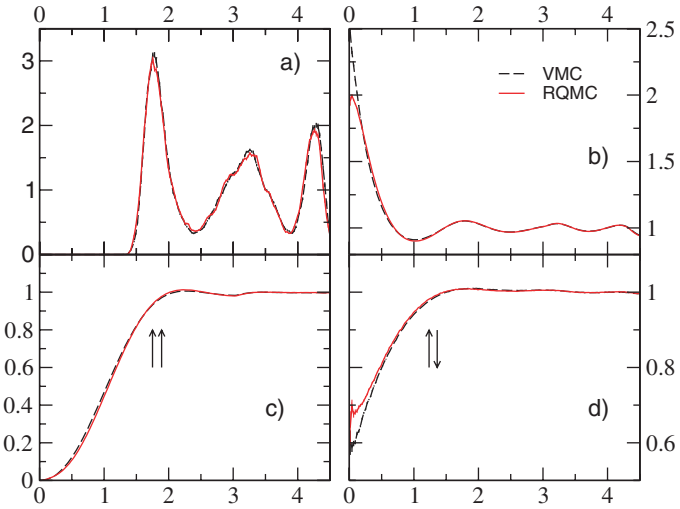

Fig. 4. $N_e = N_p = 54$, $r_s = 1.0$, $T = 1000\,\mathrm{K}$, Γ point. Comparison of VMC (*black*) and RQMC (*gray*) data for the pair correlation functions. The projection time in RQMC is $t_e = 1.0\,\mathrm{H}^{-1}$ with an electronic time step of $\tau_e = 0.02\,\mathrm{H}^{-1}$. Protons are considered as classical point particles. The proton-proton pair correlation functions exhibits a structure reminiscent of the bcc crystal structure. RQMC data for $g_{ep}(r)$ and $g_{ee}^{\uparrow\downarrow}(r)$ show a finite time step errors at short distances which however do not contribute significantly to the energy

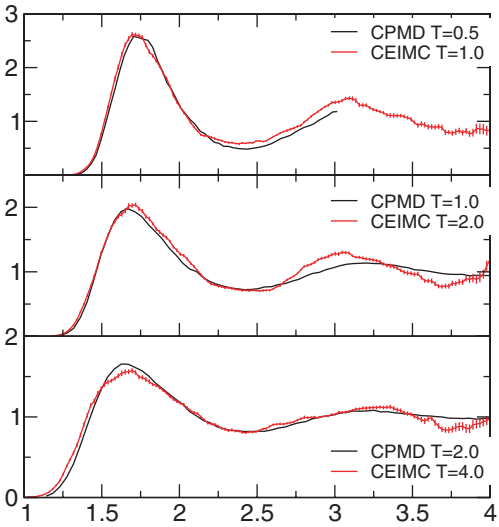

Fig. 5. Proton-proton pair correlation functions for classical protons at $r_s = 1$ and various temperatures. Comparison between CEIMC and CPMD-LDA data

$N_e = 54$ at the Γ point (zero twist angle), one at $r_s = 1.2$ and $T = 5000\,\mathrm{K}$ and the other at $r_s = 1$ and $T = 1000\,\mathrm{K}$. The comparison for the pair correlation functions are shown in Figs. 3 and 4 respectively.

It is interesting to compare the predictions of CEIMC with other methods. In refs. [16, 17] we have compared with Restricted Path Integral Monte Carlo data and with Car-Parrinello Molecular Dynamics data with LDA forces (CPMD-LDA) [54]. In Fig. 5 we compare CEIMC and CPMD-LDA $g_{pp}(r)$'s for classical protons at $r_s = 1$ and various temperatures. Both calculations are done with PBC (zero twist angle) and CEIMC uses 54 protons while CPMD-LDA used 162 protons (both are closed shells in the reciprocal space, so that the electronic ground state is not degenerate). We see that in a wide range of temperatures, CPMD-LDA and CEIMC are off by a factor of 2 in temperature. CPMD-LDA predicts a less structured fluid and locates the melting transition at roughly $T_m \simeq 350\,\mathrm{K}$ [54]. With CEIMC instead more structure is found and the melting is located between 1000 K and 1500 K [17]. Though several reasons could be at the origin of such unexpected discrepancy, we believe that the probelm arises from a too smooth BO energy surface as provided by LDA. Evidences of this fact are also provided by previous ground state calculations for hydrogen crystal structures [35] which similarly found energy differences between various structures from LDA to be roughly half of the corresponding one from DMC. This will explaine the factor of 2 in the temperature scale observed in Fig. 5.

In [17] we have reported data for the equation of state of metallic hydrogen. Proton quantum effects are quite important at such high density and need to

be considered carefully to get accurate prediction of the equation of state. The importance of proton quantum effect is partially reported in [60]. Also we have shown that electronic VMC with 3BF-A trial function is accurate enough to sample the proton configuration space. However RQMC should be used in order to obtain accurate results for the energy and the pressure. A good strategy is to run CEIMC with VMC to sample efficiently the proton configurations and then run RQMC on fixed statistical independent protonic configurations previously generated.

Insulating Molecular Hydrogen

In this section we report very preliminary results in the insulating molecular liquid phase. We have investigated the state point at $r_s = 2.1$ and $T = 4530\,\mathrm{K}$ because at this point, and other scattered points around it, experimental data for the equation of state are available from Gas-gun techniques [61]. Also the first CEIMC attempt [15,16] focused on the same point although using a quite different trial functions. We used a pair product trial function with modified RPA Jastrows (electron-electron and electron-proton) and Slater determinants built with the molecular orbitals of (55). At variance with the metallic trial function, we have now 5 variational parameters to be optimized, 4 in the Jastrow factor and a single one in the orbitals. In particular, the nodal structure of the wave function will be affected by the width of the gaussian orbitals used to build the molecular orbitals. In the first CEIMC attempt [15, 16], a single multivariate gaussian, centered at the molecular center of mass and with a width different for each molecule was used. Thus the number of variational parameter was equal to three time the number of molecules. Also, the entire optimization procedure for each attempted protonic configuration was performed prior the Metropolis test. Clearly, the optimization step was a bottleneck of that scheme. In our present scheme, we have gained evidence that we can optimize the parameters on a single protonic configuration (even the parameters optimized on a lattice configuration are good) and use the same values for simulating the liquid phase. A similar conclusion was obtained in the metallic phase with numerically optimized orbitals [16]. In this way the optimization step needs to be performed only upon changing density and/or number of particles, while we can use the same set of values for the variational parameters to span the temperature axis at fixed density and number of particles. In Fig. 6 we compare the pair correlation functions as obtained by VMC and RQMC with $\tau_e = 0.01\,\mathrm{H}^{-1}$ and $t_e = 1.6\,\mathrm{H}^{-1}$ for a system of 27 hydrogen molecules. Since the system is insulating we do not average over the twist angle, but just use the Γ point. We observe that RQMC enhances slightly the stregth of the molecular bond and the electronic correlation inside molecules with respect to VMC. Good agreement with the early CEIMC results is observed not only for the correlation function, but also for the equation of state. In our present calculation we obtain $P(RQMC) = 0.224(5)\,\mathrm{Mbars}$ to be compared with the previous estimate of $0.225(3)\,\mathrm{Mbars}$ [15, 16] and with

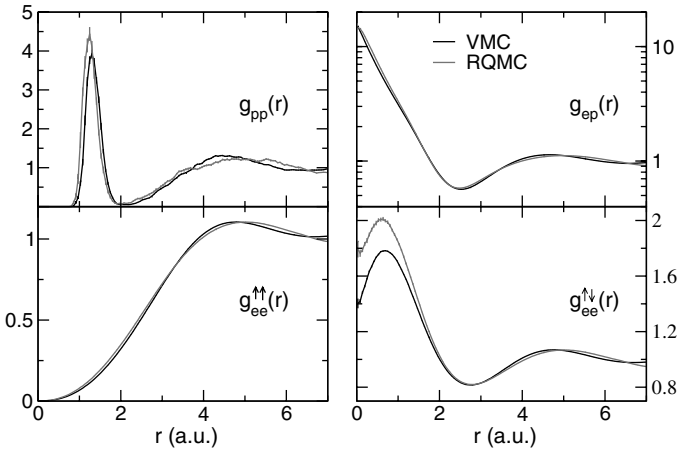

Fig. 6. Comparison between VMC and RQMC computed pair correlation functions for insulating molecular hydrogen at $r_s = 2.1, T = 4530\,\mathrm{K}$. $N_p = N_e = 54$

the experimental data $P = 0.234\,\mathrm{Mbars}$. The deviation from the experimental data is only roughly 5% and it is particularly encouraging if we consider that our data are for classical protons and quantum effects are expected to slightly increase the pressure.

6 Conclusions and Future Developments

In this paper we have described the principles of CEIMC and given some technical details on its practical implementation. The results for metallic and molecular hydrogen show that CEIMC is a practical strategy to couple ground state QMC methods for the electronic degrees of freedom with a finite temperature Monte Carlo simulation of the ionic degrees of freedom. To our knowledge, CEIMC is the only method available so far to perform ab-initio simulations based on QMC energies.

In a recent work, Grossman and Mitas have proposed a strategy to correct ab-initio Molecular Dynamics energies with QMC [62]. This is however different from CEIMC because the nuclear degrees of freedom are still sampled on the basis of DFT forces. Therefore, when applied to metallic hydrogen, that method would have found the same liquid structure as obtained by CPMD-LDA [54].

Very recently an interesting proposition on how to use noisy forces in ab-initio Molecular Dynamics has appeared [63]. The same strategy could be used with noisy QMC forces to simulate the dynamics of classical ions. A first attempt has already shown the feasibilty of this promising method [64] although the results are still very preliminary.

A crucial aspect of CEIMC is the choice of the electronic trial wave function. The ones we have discussed in this paper are either suitable for the metallic state or for the molecular state and their quality in describing the metalization-molecular dissociation transition is questionable. A current development within CEIMC is an efficient strategy to generate on the fly single electron orbitals depending on the instantaneous ionic configuration, in the spirit of the LDA orbitals previously used [35]. We have devised an efficient algorithm which is able to provide accurate orbitals in a reasonable computer time. We are at present using these orbitals to explore the molecular dissociation under pressure in the liquid state [65]. The same strategy can be used to obtain accurate prediction for the hydrogen equation of state in the temperature range between 50 K and 5000 K. Also application to helium and helium-hydrogen mixtures, very interesting systems for planetary physics, can be envisaged with the same methodology.

Tests for non-hydrogenic systems are needed to find the performance of the method on a broader spectrum of applications. The use of pseudopotentials within QMC to treat atoms with inner core is well tested [6]. What is not clear is how much time will be needed to generate trial functions, and to reduce the noise level to acceptable limits. Clearly, further work is needed to allow this next step in the development of microscopic simulation algorithms.

References

1. R. Car and M. Parrinello (1985) Unified Approach for Molecular Dynamics and Density-Functional Theory. *Phys. Rev. Letts.* **55**, p. 2471
2. M. Bernasconi, G. L. Chiarotti, P. Focher, S. Scandolo, E. Tosatti, and M. Parrinello (1995) First-principle-constant pressure molecular dynamics. *J. Phys. Chem. Solids* **56**, p. 501
3. A. Alavi, J. Kohanoff, M. Parrinello, and D. Frenkel (1994) Ab Initio Molecular Dynamics with Excited Electrons. *Phys. Rev. Letts.* **73**, pp. 2599–2602
4. D. Marx and M. Parrinello (1996) Ab initio path integral molecular dynamics: Basic ideas. *J. Chem. Phys.* **104**, p. 4077
5. R. M. Martin (2004) Electronic Structure. Basic Theory and Practical Methods. Cambridge University Press, Cambridge
6. M. W. C. Foulkes, L. Mitas, R. J. Needs, and G. Rajagopal (2001) Quantum Monte Carlo simulations of solids. *Rev. Mod. Phys.* **73**, p. 33
7. E. G. Maksimov and Y. I. Silov (1999) Hydrogen at high pressure. *Physics-Uspekhi* **42**, p. 1121
8. M. Stadele and R. M. Martin (2000) Metallization of Molecular Hydrogen: Predictions from Exact-Exchange Calculations. *Phys. Rev. Lett.* **84**, pp. 6070–6073
9. K. A. Johnson and N. W. Ashcroft (2000) Structure and bandgap closure in dense hydrogen. *Nature* **403**, p. 632
10. D. Alfé, M. Gillan, M. D. Towler, and R. J. Needs (2004) Efficient localized basis set for quantum Monte Carlo calculations on condensed matter. *Phys. Rev. B* **70**, p. 161101

11. B. L. Hammond, W. A. Lester Jr., and P. J. Reynolds (1994) Monte Carlo methods in Ab Initio Quantum Chemistry. World Scientific Singapore
12. R. M. Panoff and J. Carlson (1989) Fermion Monte Carlo algorithms and liquid 3He. *Phys. Rev. Letts.* **62**, p. 1130
13. Y. Kwon, D. M. Ceperley, and R. M. Martin (1994) Quantum Monte Carlo calculation of the Fermi-liquid parameters in the two-dimensional electron gas. *Phys. Rev. B* **50**, pp. 1684–1694
14. M. Holzmann, D. M. Ceperley, C. Pierleoni, and K. Esler (2003) Backflow correlations for the electron gas and metallic hydrogen. *Phys. Rev. E* **68**, p. 046707[1–15]
15. M. Dewing and D. M. Ceperley (2002) Methods in Coupled Electron-Ion Monte Carlo. In *Recent Advances in Quantum Monte Carlo Methods II* (Ed. S. Rothstein), World Scientific
16. D. M. Ceperley, M. Dewing, and C. Pierleoni (2002) The Coupled Electronic-Ionic Monte Carlo Simulation Method. *Lecture Notes in Physics* **605**, pp. 473–499, Springer-Verlag; physics/0207006
17. C. Pierleoni, D. M. Ceperley, and M. Holzmann (2004) Coupled Electron-Ion Monte Carlo Calculations of Dense Metallic Hydrogen. *Phys. Rev. Lett.* **93**, 146402[1–4]
18. S. Baroni and S. Moroni (1999) Reptation Quantum Monte Carlo: A Method for Unbiased Ground-State Averages and Imaginary-Time Correlations. *Phys. Rev. Letts.* **82**, pp. 4745–4748; S. Baroni, S. Moroni *Reptation quantum Monte Carlo* in "Quantum Monte Carlo Methods in Physics and Chemistry", eds. M. P. Nightingale and C. J. Umrigar (Kluwer, 1999), p. 313
19. D. M. Ceperley (1995) Path integrals in the theory of condensed helium. *Rev. Mod. Phys.* **67**, pp. 279–355
20. A. Sarsa, K. E. Schmidt, and W. R. Magro (2000) A path integral ground state method. *J. Chem. Phys.* **113**, p. 1366
21. R. P. Feynman (1998) Statistical Mechanics: a set of lectures. Westview Press
22. K. Huang (1988) Statistical Mechanics, John Wiley
23. S. Zhang and H. Krakauer (2003) Quantum Monte Carlo Method using Phase-Free Random Walks with Slater Determinants. *Phys. Rev. Lett.* **90**, p. 136401
24. R. W. Hall (2005) Simulation of electronic and geometric degrees of freedom using a kink-based path integral formulation: Application to molecular systems. *J. Chem. Phys.* **122**, p. 164112[1–8]
25. A. J. W. Thom and A. Alavi (2005) A combinatorial approach to the electron correlation problem. *J. Chem. Phys.* in print
26. D. M. Ceperley (1996) Path integral Monte Carlo methods for fermions. In *Monte Carlo and Molecular Dynamics of Condensed Matter Systems*, ed. by K. Binder and G. Ciccotti, Editrice Compositori, Bologna, Italy
27. D. M. Ceperley (1991) Fermion Nodes. *J. Stat. Phys.* **63**, p. 1237
28. D. Bressanini, D. M. Ceperley, and P. Reynolds (2001) What do we know about wave function nodes?. In *Recent Advances in Quantum Monte Carlo Methods II*, ed. S. Rothstein, World Scientfic
29. G. Ortiz, D. M. Ceperley, and R. M. Martin (1993) New stochastic method for systems with broken time-reversal symmetry: 2D fermions in a magnetic field. *Phys. Rev. Lett.* **71**, p. 2777
30. C. Lin, F. H. Zong, and D. M. Ceperley (2001) Twist-averaged boundary conditions in continuum quantum Monte Carlo algorithms. *Phys. Rev. E* **64**, 016702[1–12]

31. G. Ortiz and D. M. Ceperley (1995) Core Structure of a Vortex in Superfluid 4He. *Phys. Rev. Lett.* **75**, p. 4642
32. V. D. Natoli (1994) A Quantum Monte Carlo study of the high pressure phases of solid hydrogen, Ph.D. Theses, University of Illinois at Urbana-Champaign.
33. D. M. Ceperley and B. J. Alder (1987) Ground state of solid hydrogen at high pressures. *Phys. Rev. B* **36**, p. 2092
34. X. W. Wang, J. Zhu, S. G. Louie, and S. Fahy (1990) Magnetic structure and equation of state of bcc solid hydrogen: A variational quantum Monte Carlo study. *Phys. Rev. Lett.* **65**, p. 2414
35. V. Natoli, R. M. Martin, and D. M. Ceperley (1993) Crystal structure of atomic hydrogen. *Phys. Rev. Lett.* **70**, p. 1952
36. V. Natoli, R. M. Martin, and D. M. Ceperley (1995) Crystal Structure of Molecular Hydrogen at High Pressure. *Phys. Rev. Lett.* **74**, p. 1601
37. C. Pierleoni and D. M. Ceperley (2005) Computational methods in Coupled Electron-Ion Monte Carlo. *Chem. Phys. Chem.* **6**, p. 1872
38. D. Ceperley (1986) The Statistical Error of Green's Function Monte Carlo, in Proceedings of the Metropolis Symposium on. The Frontiers of Quantum Monte Carlo. *J. Stat. Phys.* **43**, p. 815
39. D. M. Ceperley and M. H. Kalos (1979) Monte Carlo Methods in Statistical Physics, ed. K. Binder, Springer-Verlag.
40. D. M. Ceperley, G. V. Chester, and M. H. Kalos (1977) Monte Carlo simulation of a many-fermion study. *Phys. Rev. B* **16**, p. 3081
41. D. M. Ceperley and B. J. Alder (1984) Quantum Monte Carlo for molecules: Green's function and nodal release. *J. Chem. Phys.* **81**, p. 5833
42. C. Pierleoni, K. Delaney, and D. M. Ceperley, to be published
43. D. Frenkel and B. Smit (2002) Understanding Molecular Simulations: From Algorithms to Applications, 2nd Ed., Academic Press, San Diego
44. S. Moroni, private communication
45. D. M. Ceperley and M. Dewing (1999) The penalty method for random walks with uncertain energies. *J. Chem. Phys.* **110**, p. 9812
46. I. F. Silvera and V. V. Goldman (1978) The isotropic intermolecular potential for H2 and D2 in the solid and gas phases. *J. Chem. Phys.* **69**, p. 4209
47. W. Kolos and L. Wolniewicz (1964) Accurate Computation of Vibronic Energies and of Some Expectation Values for H2, D2, and T2. *J. Chem. Phys.* **41**, p. 3674
48. E. Babaev, A. Sudbo, and N. W. Ashcroft (2004) A superconductor to superfluid phase transition in liquid metallic hydrogen. *Nature* **431**, p. 666
49. I. F. Silvera (1980) The solid molecular hydrogens in the condensed phase: Fundamentals and static properties. *Rev. Mod. Phys.* **52**, p. 393
50. C. Pierleoni, D. M. Ceperley, B. Bernu, and W. R. Magro (1994) Equation of State of the Hydrogen Plasma by Path Integral Monte Carlo Simulation. *Phys. Rev. Lett.* **73**, p. 2145; W. R. Magro, D. M. Ceperley, C. Pierleoni and B. Bernu (1996) Molecular Dissociation in Hot, Dense Hydrogen. *Phys. Rev. Lett.* **76**, p. 1240
51. B. Militzer and D. M. Ceperley (2000) Path Integral Monte Carlo Calculation of the Deuterium Hugoniot. *Phys. Rev. Lett.* **85**, p. 1890
52. B. Militzer and D. M. Ceperley (2001) Path integral Monte Carlo simulation of the low-density hydrogen plasma. *Phys. Rev. E* **63**, p. 066404
53. D. Hohl, V. Natoli, D. M. Ceperley, and R. M. Martin (1993) Molecular dynamics in dense hydrogen. *Phys. Rev. Lett.* **71**, p. 541

54. J. Kohanoff and J. P. Hansen (1995) Ab Initio Molecular Dynamics of Metallic Hydrogen at High Densities. *Phys. Rev. Lett.* **74**, pp. 626–629; *ibid.* (1996) Statistical properties of the dense hydrogen plasma: An ab initio molecular dynamics investigation. *Phys. Rev. E* **54**, pp. 768–781
55. J. Kohanoff, S. Scandolo, G. L. Chiarotti, and E. Tosatti (1997) Solid Molecular Hydrogen: The Broken Symmetry Phase. *Phys. Rev. Lett.* **78**, p. 2783
56. S. Scandolo (2003) Liquid-liquid phase transition in compressed hydrogen from first-principles simulations. *PNAS* **100**, p. 3051
57. S. A. Bonev, E. Schwegler, T. Ogitsu, and G. Galli (2004) A quantum fluid of metallic hydrogen suggested by first-principles calculations. *Nature* **431**, p. 669
58. S. T. Weir, A. C. Mitchell, and W. J. Nellis (1996) Metallization of Fluid Molecular Hydrogen at 140 GPa (1.4 Mbar). *Phys. Rev. Lett.* **76**, p. 1860
59. T. Guillot, G. Chabrier, P. Morel, and D. Gautier (1994) Nonadiabatic models of Jupiter and Saturn. *Icarus* **112**, p. 354; T. Guillot, P. Morel (1995) Coupled Electron Ion Monte Carlo Calculations of Atomic Hydrogen. *Astron. & Astrophys. Suppl.* **109**, p. 109
60. M. Holzmann, C. Pierleoni, and D. M. Ceperley (2005) Coupled Electron Ion Monte Carlo Calculations of Atomic Hydrogen. *Comput. Physics Commun.* **169**, p. 421
61. N. C. Holmes, M. Ross, and W. J. Nellis (1995) Temperature measurements and dissociation of shock-compressed liquid deuterium and hydrogen. *Phys. Rev. B* **52**, p. 15835
62. J. C. Grossman, L. Mitas (2005) Efficient Quantum Monte Carlo Energies for Molecular Dynamics Simulations. *Phys. Rev. Lett.* **94**, p. 056403
63. F. Krajewski and M. Parrinello (2005) Stochastic linear scaling for metals and nonmetals. *Phys. Rev. B* **71**, p. 233105; F. Krajewski, M. Parrinello, Linear scaling electronic structure calculations and accurate sampling with noisy forces. cond-mat/0508420
64. C. Attaccalite (2005) RVB phase of hydrogen at high pressure:towards the first ab-initio Molecular Dynamics by Quantum Monte Carlo, Ph.D. theses, SISSA-Trieste.
65. K. Delaney, C. Pierleoni and D.M. Ceperley (2006) Quantum Monte Carlo Simulation of the High-Pressure Molecular-Atomic Transition in Fluid Hydrogen. cond-mat/0603750, submitted to Phys. Rev. Letts.,